Glass compositions and tempo of post-17 ka eruptions from the Afar Triangle recorded in sediments from lakes Ashenge and Hayk, Ethiopia

Martin-Jones, Catherine Mariel; Lane, Christine; Pearce, Nicholas; Smith, Victoria C.; Lamb, Henry; Oppenheimer, Clive; Asrat, Asfawossen; Schaebitz, Frank

Published in:
Quaternary Geochronology

DOI:
10.1016/j.quageo.2016.10.001

Publication date:
2017

Citation for published version (APA):
Martin-Jones, C. M., Lane, C., Pearce, N., Smith, V. C., Lamb, H., Oppenheimer, C., Asrat, A., & Schaebitz, F. (2017). Glass compositions and tempo of post-17 ka eruptions from the Afar Triangle recorded in sediments from lakes Ashenge and Hayk, Ethiopia. *Quaternary Geochronology*, *37*, 15-31. https://doi.org/10.1016/j.quageo.2016.10.001

Quaternary Geochronology 37 (2017) 15–31

Contents lists available at ScienceDirect

Quaternary Geochronology

journal homepage: www.elsevier.com/locate/quageo

Glass compositions and tempo of post-17 ka eruptions from the Afar Triangle recorded in sediments from lakes Ashenge and Hayk, Ethiopia

C.M. Martin-Jones [a, *], C.S. Lane [b], N.J.G. Pearce [a], V.C. Smith [c], H.F. Lamb [a], C. Oppenheimer [b], A. Asrat [d], F. Schaebitz [e]

[a] Department of Geography and Earth Sciences, Aberystwyth University, Aberystwyth, SY23 3DB, UK
[b] Department of Geography, University of Cambridge, Downing Place, Cambridge, CB2 3EN, UK
[c] Research Laboratory for Archaeology and the History of Art, University of Oxford, Oxford, OX1 3QY, UK
[d] School of Earth Sciences, Addis Ababa University, P.O. Box 1176, Addis Ababa, Ethiopia
[e] Institute of Geography Education, University of Cologne, 50931, Köln, Germany

ARTICLE INFO

Article history:
Received 18 March 2016
Received in revised form
20 September 2016
Accepted 13 October 2016
Available online 18 October 2016

Keywords:
Tephrochronology
Afar
Glass chemistry
Eruption history

ABSTRACT

Numerous volcanoes in the Afar Triangle and adjacent Ethiopian Rift Valley have erupted during the Quaternary, depositing volcanic ash (*tephra*) horizons that have provided crucial chronology for archaeological sites in eastern Africa. However, late Pleistocene and Holocene tephras have hitherto been largely unstudied and the more recent volcanic history of Ethiopia remains poorly constrained. Here, we use sediments from lakes Ashenge and Hayk (Ethiopian Highlands) to construct the first <17 cal ka BP tephrostratigraphy for the Afar Triangle. The tephra record reveals 21 visible and crypto-tephra layers, and our new database of major and trace element glass compositions will aid the future identification of these tephra layers from proximal to distal locations. Tephra compositions include comendites, pantellerites and minor peraluminous and metaluminous rhyolites. Variable and distinct glass compositions of the tephra layers indicate they may have been erupted from as many as seven volcanoes, most likely located in the Afar Triangle. Between 15.3–1.6 cal. ka BP, explosive eruptions occurred at a return period of <1000 years. The majority of tephras are dated at 7.5–1.6 cal. ka BP, possibly reflecting a peak in regional volcanic activity. These findings demonstrate the potential and necessity for further study to construct a comprehensive tephra framework. Such tephrostratigraphic work will support the understanding of volcanic hazards in this rapidly developing region.

1. Introduction

1.1. Geological setting

The Afar Triangle of northern Ethiopia represents one of the best examples of an active rifting system on Earth, marking the juxtaposition of the Arabian, Somalian and African plates above a mantle plume (Schilling, 1973; Mohr, 1978). During the Quaternary, explosive eruptions occurred at many volcanoes in the Afar Triangle and the adjacent Ethiopian Rift Valley (Pyle, 1999). Volcanic ash (*tephra*) ejected by explosive eruptions may be dispersed over ranges of hundreds or thousands of kilometres, forming widespread chronostratigraphic markers in sedimentary archives. Pleistocene tephras have been correlated throughout Ethiopia, Kenya and the Gulf of Aden and have been crucial in providing chronological control for regional palaeoanthropological sites (e.g. Brown, 1982; Pickford et al., 1991; WoldeGabriel et al., 1999; Katoh et al., 2000; Clark et al., 2003; Brown et al., 2006; Haile-Selassie et al., 2007; Campisano and Feibel, 2008; DiMaggio et al., 2008; Saylor et al., 2016).

Regional volcanic activity has continued into the Holocene. However, of the ~40 Holocene volcanoes in the Afar Triangle, very few have recorded historical eruptions (Siebert et al., 2011). Recent explosive volcanism has occurred from the Nabro Volcanic Range (Goitom et al., 2015), which extends ~110 km across the northern Afar towards the Red Sea (Fig. 1a). The Dubbi volcano (Eritrea), located along the same volcanic lineament, was home to Africa's largest historical eruption. The AD 1861 eruption dispersed volcanic ash ~300 km to the west, towards the Ethiopian Highlands, and the eruption culminated with the effusion of ~3.5 km^3 of basaltic lava.

* Corresponding author.
E-mail address: martinjonescatherine@gmail.com (C.M. Martin-Jones).

http://dx.doi.org/10.1016/j.quageo.2016.10.001

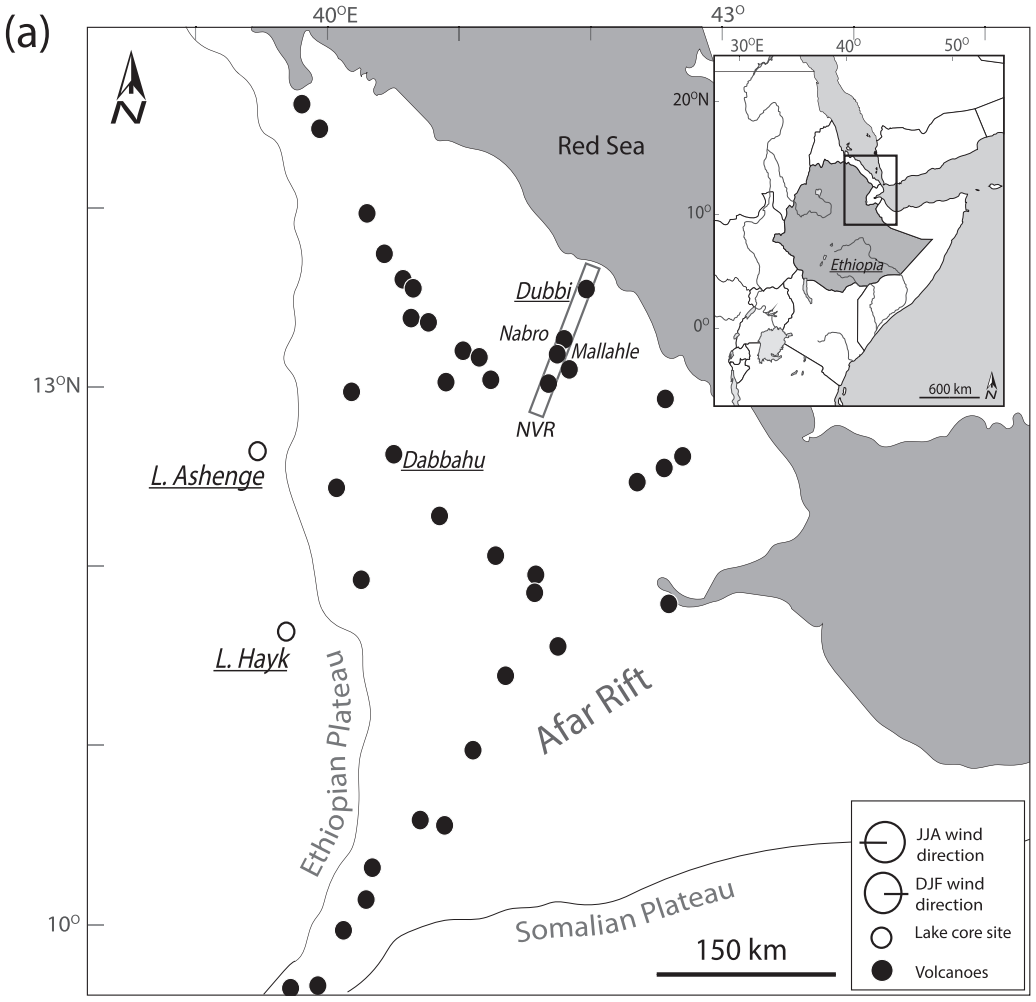
(a)
40°E
43°
30°E
40°
50°
20°N
10°
0°
13°N
10°
Red Sea
Ethiopia
600 km
Dubbi
Nabro
Mallahle
NVR
Dabbahu
L. Ashenge
L. Hayk
Afar Rift
Ethiopian Plateau
Somalian Plateau
150 km
JJA wind direction
DJF wind direction
Lake core site
Volcanoes

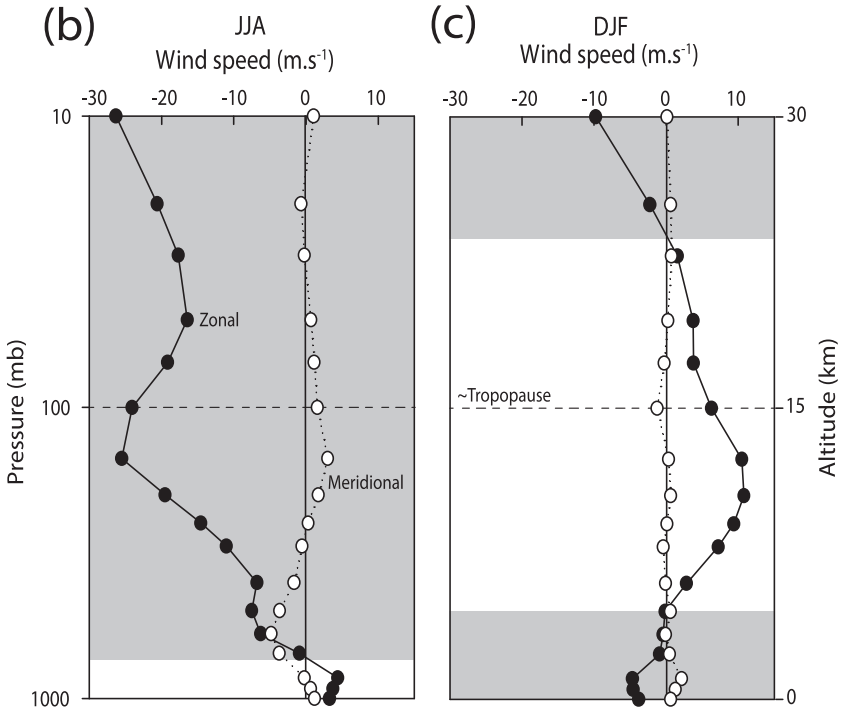
(b)
JJA
Wind speed (m.s-1)
-30
-20
-10
0
10
10
100
1000
Pressure (mb)
Zonal
Meridional
(c)
DJF
Wind speed (m.s-1)
-30
-20
-10
0
10
30
15
0
Altitude (km)
~Tropopause

Proximal ignimbrite and pumice deposits from the AD 1861 eruption are trachytic to rhyolitic in composition (Wiart and Oppenheimer, 2004). An eruption witnessed from the Red Sea in AD 1400 may also have been derived from the Dubbi volcano (Gouin, 1979).

Nabro volcano (Eritrea) itself forms a double caldera with the neighbouring volcano, Mallahle (Fig. 1a). The volcano is constructed from trachytic pyroclastic deposits and lava flows, with rhyolitic obsidian domes and trachybasaltic flows inside the caldera (Wiart and Oppenheimer, 2004). The formation of this caldera most likely represents the largest explosive eruption in northern Afar during the Quaternary, which may have produced a widespread tephra (Wiart and Oppenheimer, 2004). The first recorded eruption of Nabro in 2011 (VEI = 4) dispersed volcanic ash over Africa and Eurasia, disrupting air traffic. At the time of the eruption no volcanic monitoring network existed, so there was no warning (Goitom et al., 2015).

Located to the west of the Nabro Volcanic Range and closer to the Rift shoulders, Dabbahu (Ethiopia) (Fig. 1a) is a Pleistocene-Holocene volcanic massif. The Dabbahu volcanic products have evolved through fractional crystallisation dominated by K-feldspar, clinopyroxene and apatite to produce a basalt-pantellerite suite (Barberi et al., 1975; Field et al., 2012). Fission track dates on obsidians from the upper flanks give ages of ~44 ka and ~1.5 ka. An eruption (VEI = 3) in 2005 deposited tephra over 100 km^2 and formed a small rhyolitic lava dome (Ayele et al., 2007a; Ferguson et al., 2010).

Recent studies, including the Ethiopia-Afar Geoscientific Lithospheric Experiment (EAGLE) and Afar Rift Consortium, have provided a wealth of information on magmatic and tectonic processes in the Afar (e.g. Ayele et al., 2007b; Bastow et al., 2011; Keir et al., 2011; Ferguson et al., 2013). However, late Pleistocene and Holocene tephra deposits in the Afar are yet to be systematically studied and the recent eruptive history of the region remains poorly constrained, due in part to the logistical difficulties of undertaking fieldwork in this remote area.

1.2. Distal tephra records

Distal tephra, including lacustrine and marine, records give insight into the frequency of past eruptions from a range of sources, which provides information on the likelihood of future activity. These records often provide more comprehensive and accessible records of long-term volcanism, whereas outcrops near volcanoes may be poorly exposed, buried or eroded, or have no clear stratigraphic context (e.g. Rawson et al., 2015). For example, the record of Lago Grande di Monticchio in Italy has been used to constrain the tempo of Italian volcanism, especially that of Ischia (Wulf et al., 2004; Tomlinson et al., 2014). Furthermore, marine cores off the coast of Monserrat have been used to obtain long-term records of activity and assess the link to variations in sea level (Coussens et al., 2016). To date, few studies have used east African lake sediments to investigate past eruption frequency. However, marine tephra records from the Indian Ocean and the Gulf of Aden have provided valuable information on the timing and magnitude of Oligocene eruptions from the Afro-Arabian flood volcanic province and Plio-Pleistocene events from the East African Rift System (Ukstins Peate et al., 2003; Feakins et al., 2007).

Furthermore, lake sediments have good potential for radiocarbon dating and these dates can be used in conjunction with stratigraphic information in Bayesian age models, e.g. OxCal (Bronk Ramsey, 2009a), to further constrain the ages of the events (e.g. Rawson et al., 2015).

Prior to interpreting distal records of past volcanic activity, it is important to consider factors that may determine the flux of tephras to individual sites and their subsequent preservation. These factors include eruption magnitude and intensity, wind speed and direction, and the grain-size of ejecta (Sparks et al., 1997). The wind direction varies seasonally over Ethiopia (Fig. 1) and this will determine the dispersal of tephra and consequently the likelihood of it being preserved in a distal record. During the winter, easterly winds may disperse tephra from volcanoes in the Afar towards the Ethiopian Highlands (Fig. 1b and c); whilst, during the summer the winds reverse causing tephra produced in the Afar to be predominantly dispersed to the east. However, these are modern wind regimes which may have changed over the late Quaternary. On an individual site basis, processes including sediment focussing, bioturbation, slumping and tectonic movement may compromise the stratigraphic position, and therefore the apparent age, of a tephra layer (e.g. Payne and Gehrels, 2010), causing misinterpretation of past eruption tempo. Despite these challenges, our research demonstrates the great potential to achieve a detailed understanding of the composition and tempo of late Pleistocene to Holocene explosive volcanism in Ethiopia via the investigation of lacustrine records.

1.3. Research aims

This research aims to produce the first detailed lake sediment tephra record from lakes Ashenge and Hayk (Ethiopian Highlands), spanning <17 cal. ka BP (Fig. 1a). This initial tephra record will provide the most complete assessment of explosive eruption frequency and tephra dispersal from the Afar during the late Pleistocene and Holocene so far available.

This study involves the identification of both visible volcanic ash (tephra) layers and crypto-tephra layers - fine grained and dilute tephras that cannot be identified in the host sediments by the naked eye (e.g. Lane et al., 2014; Davies, 2015). Using glass shard compositions and Bayesian age-modelling techniques, our study provides the first reference dataset for comparison with tephra deposits in the region. Our findings demonstrate the great potential for building upon these records and better evaluating volcanic hazards by using this distal lake sediment stratigraphic approach.

2. Materials and methods

2.1. Lake core and proximal tephra sampling

Lakes Ashenge and Hayk are located on the flank of the Ethiopian Highlands, <70 km from Holocene volcanoes in the Afar Triangle. Lake Ashenge is located in a graben consisting of mid-Tertiary basalts at an elevation of 2500 m a.s.l and has a maximum water depth of ~20 m (Marshall et al., 2009). An 8 m long sediment core (03AL3/2) was extracted from the lake using a Livingstone Piston Corer in 2003, at a water depth of 9 m. Lake Hayk has a maximum depth of 88 m and is situated at 1900 m a.s.l. in an

Fig. 1. (a) Map of the Afar (N Ethiopia) showing the location of lakes Ashenge and Hayk and Holocene volcanoes (Siebert et al., 2011). Volcanoes referred to in the text are labelled, NVR = Nabro Volcanic Range. (b) Profile through atmosphere showing the speed of zonal and meridional winds during the summer and (c) winter monsoon months, after Feakins et al. (2007). Wind velocities are from the NOAA NCEP CDAS-1 monthly pressure level climatology dataset spanning January 1949–January 2016 (Kalnay et al., 1996), averaged over 40–45°E, 10–15°N. Favourable wind directions for transporting tephra to the Ethiopian Highlands are shaded in grey, negative (positive) wind speed values indicate easterly (westerly) flow of zonal winds and southerly (northerly) flow of meridional winds.

extensional basin developed in Miocene to early Pliocene basalts, tuffs and rhyolitic lava flows (Ghinassi et al., 2012). A 7.5 m long sediment core (Hayk-01-2010) was extracted from the lake in 2010 at a water depth of 78 m, using a UWITEC corer.

Proximal samples from the Dubbi Volcano have been analysed in this study to ascertain whether this is the source for some of the distal tephras deposited in lakes Ashenge and Hayk. Pyroclastic flow deposits associated with the Dubbi AD 1861 eruption were sampled 12 km to the southwest of the vent at 13° 30′53″N, 41° 42′48″E (samples c and y in Wiart and Oppenheimer (2000)).

2.2. Visible tephra sampling and cryptotephra identification

The physical properties, depths and thicknesses of visible tephras in the Ashenge and Hayk sediments were recorded and sampled. Samples (~2 cm^3) were taken from the full thickness of visible tephra layers; were wet sieved and the 90–250 μm fraction was used for analysis.

To locate cryptotephras, the standard extraction methods detailed in Blockley et al. (2005) were followed. This method allows for the extraction and identification of glass shards that are silica-rich in composition. Given that most large explosive eruptions are from evolved systems that are silica-rich, this method is appropriate for identifying widespread tephra layers. However, volcanism in the Afar and Main Ethiopian Rift is bimodal (Peccerillo et al., 2003, 2007) and there may also be a number of basaltic units that have not been investigated in this study.

Contiguous and continuous samples were collected from the sediment at 10 cm intervals, however samples were not taken from depths at which visible tephras occur. Samples were dried, weighed and treated with 1 M HCl to remove carbonates, then sieved to >25 μm and density separated to 1.95–2.55 g/cm^3. Glass shards isolated from the host sediments were then counted under a transmitted light microscope. Regions of sediment containing elevated shard concentrations (>300 shards per 0.25 g of dried sediment) were re-sampled at a 1 cm resolution, reprocessed and the extracted shards counted to identify the stratigraphic position of the cryptotephra horizon. Visible and crypto-tephras containing high concentrations of glass shards (>100,000 shards per 0.25 g of dried sediment) clearly exceeding background levels were numbered as Ashenge Tephra layers (AST) 1–9. Peaks associated with lower shard concentrations (<100,000 shards per 0.25 g of dried sediment) were not explored further in this study. If crypto-tephras are reworked, glass shards may be dispersed throughout the stratigraphy. Primary cryptotephra deposits are typically characterised by a rapid basal rise in the concentration of glass shards, which then decline upwards through the stratigraphy (Davies et al., 2012). Samples for geochemical analysis were taken at the depth of the initial increase in shard counts in the stratigraphy.

2.3. Glass compositional analysis

Glass shards from visible and crypto-tephras were mounted in epoxy resin and the internal surfaces exposed and polished. Single grain major and minor element concentrations were measured using a Jeol 8600 wavelength dispersive electron microprobe (EMPA) at the Research Laboratory for Archaeology and the History of Art, University of Oxford. To reduce alkali migration in the glass a defocussed beam with a 10 μm diameter, 15 kV accelerating voltage and 6 nA beam current was used. Sodium was collected for 10 s, Cl and P were collected for 60 s and other major elements were collected for 30 s. A suite of mineral standards were used to calibrate the instrument, and the MPI-DING volcanic glasses (Jochum et al., 2006) were used as secondary standards. All analyses presented in the text, tables and graphs have been normalised to an anhydrous basis, to remove the effects of variable secondary hydration in the glasses (e.g. Pearce et al., 2008). Raw data and secondary standard analyses can be found in the Supplementary Information (S1).

Trace element compositions of single glass shards were determined using laser ablation (LA) ICP-MS at Aberystwyth University. Analyses were performed using a Coherent GeoLas ArF 193 nm Excimer laser coupled to a Thermo Finnigan Element 2 ICP-MS, with a laser energy of 10 J cm^{-2}, repetition rate of 5 Hz and 24 s acquisition time. The minor ^{29}Si isotope was used as the internal standard, the SiO_2 content having previously been determined by EPMA. Trace element concentrations (ppm) were calculated by comparing the analyte isotope intensity/internal standard intensity in the shard to the same ratio in the NIST SRM 612 reference material using published concentrations from Pearce et al. (1997). Analyses using <20 μm spot sizes were corrected for variations in element fractionation (Pearce et al., 2011). The rhyolitic MPI-DING reference material, ATHO-G, was analysed during each analytical run to monitor accuracy and precision; these analyses are given in the Supplementary Information (S1).

This study tests the potential for tephra correlations between lakes Ashenge and Hayk primarily using selected major and trace element bi-plots. Compositional similarities were further tested using principal component analysis (PCA). Yttrium, Zr, Nb, Ba, La and Th, were selected as variables for the PCA, these elements having shown the most variability in bi-plots.

2.4. Chronology

To assess eruption frequency, age models were constructed for each record, using a combination of new and published (Marshall et al., 2009) radiocarbon dates on bulk sediment samples (Table 1). New radiocarbon dates (n=7) on the Ashenge sediments were undertaken at the Scottish Universities Environmental Research Centre (SUERC) accelerator mass spectrometry (AMS) Laboratory. Radiocarbon dates (n=14) on the Hayk sediments were undertaken at the Oxford Radiocarbon Accelerator Unit, University of Oxford, and the 14 CHRONO Centre, Queen's University Belfast.

Organic-rich bulk sediment samples for radiocarbon dating were digested in 2 M HCl for 8 h at 80° C, washed with distilled water and homogenised. Pre-treated samples were heated with CuO in sealed plastic tubes to recover the CO_2, which was then converted to graphite by Fe/Zn reduction. The radiocarbon was then measured using AMS.

All radiocarbon ages were calibrated using IntCal13 (Reimer et al., 2013). Bayesian P_Sequence depositional models were run for both sequences, using OxCal version 4.2 (Bronk Ramsey, 2009a) with outlier analysis (Bronk Ramsey, 2009b). Interpolated tephra ages were retrieved using the *Date* function and are quoted herein as 95.4% confidence intervals. Prior to analysis, sediment depths were converted to event free depths that do not include tephras of >0.5 cm thickness, which are presumed to have been deposited instantaneously. Due to the presence of a significant hiatus at around 650 cm depth in the Lake Ashenge 03AL3/2 stratigraphy, separate P_Sequence age models were run to model the sediment deposition above and below this point. Full details, along with the OxCal code, for each age model can be found in the Supplementary Information (S2).

3. Results

3.1. Tephrochronology of the Ashenge sediments

The Lake Ashenge sediments contain 9 tephras, labelled here AST-1 to AST-9 (youngest to oldest) and ranging in age from

Table 1
AMS ^{14}C measurements for the Ashenge and Hayk lake sediment cores. All analyses were undertaken on bulk sediment samples. Dates on Ashenge sediments from Marshall et al. (2009) are indicated in bold. Ages were calibrated using IntCal13 (Reimer et al., 2013) run in OxCal version 4.2 (Bronk Ramsey, 2009a). * Sample SUERC-7178 from 645.5 cm depth was re-analysed (SUERC-7439) using archived CO_2 from original sample, both dates have been combined using the *R_Combine* function.

Laboratory number	^{14} C ages a (±1 σ)	depth (cm)	δ^{13} C (‰ PDB)	Calibrated ages a BP
Ashenge				
SUERC-29473	378 ± 37	3.5	−22.6	507–316
SUERC-6263	618 ± 31	51.5	−20.9	658–550
SUERC-29476	923 ± 35	104.5	−21.7	927–776
SUERC-6264	1609 ± 22	175.5	−24.0	1553–1415
SUERC-29477	2082 ± 37	246.5	−24.4	2150–1951
SUERC-6265	2865 ± 28	300.5	−23.0	3069–2883
SUERC-29478	3298 ± 35	341.5	−22.0	3611–3450
SUERC-29479	4143 ± 38	386.5	−22.2	4808–4527
SUERC-6266	4714 ± 30	440.5		5581–5324
SUERC-29480	4361 ± 38	485.5	−23.6	5039–4852
SUERC-6268	5063 ± 34	551.5	−22.1	5907–5741
SUERC-29481	5671 ± 39	600.5	−22.5	6564–6324
SUERC-7178	6696 ± 40	645.5	−20.8	7581–7476
SUERC-7439 *	6622 ± 40	645.5		*7581–7476*
SUERC-6269	10127 ± 66	657	−23.4	12015–11398
Beta-187297	11920 ± 40	739.5	−25.1	13961–13574
SUERC-6270	12810 ± 99	771.5	−21.3	15675–15005
Hayk				
UBA-27072	1583 ± 32	12.5		1546–1395
OxA-30960	2485 ± 32	100	−23.4	2729–2434
OxA-30883	2795 ± 31	140	−23	2974–2796
UBA-25092	3563 ± 36	172		3973–3724
OxA-30885	4068 ± 33	183	−23.1	4802–4436
OxA-30886	4914 ± 35	196	−23.6	5717–5591
OxA-30887	7650 ± 45	240	−24.2	8541–8383
UBA-27073	9643 ± 79	314.5		11193–10722
UBA-27074	10102 ± 44	396.5		11987–11415
UBA-25093	10393 ± 45	429		12237–11838
UBA-25094	10287 ± 46	442		12368–12020
UBA-27075	10254 ± 62	447.5		12383–12029
UBA-27076	12846 ± 67	657.5		15465–15069
UBA-25095	12873 ± 60	717.5		15726–15261

15.3–0.3 cal. ka BP (Table 2). Five cryptotephras (AST-3; 4; 6; 7 and 9), containing high glass shard concentrations (>1000 shards per 0.25 g of dried sediment), were identified through density separation techniques (Fig. 2). Visible tephras (AST-1; 2; 5 and 8) are grey-white in colour, normally graded and range in thickness from 1.0–2.5 cm and in grain-size from coarse to fine volcanic ash.

The youngest tephra (AST-1) dates to the historical period, between 546–321 cal. a BP (AD 1404–1629) (Fig. 2). This eruption followed a >4 ka interval during which no tephras were deposited at Lake Ashenge. Between ~7.5–~4.8 cal. ka BP 6 tephra layers were recorded (AST-2 to AST-7). Below the hiatus in the sediment record, 2 more tephra layers (AST-8 to AST-9) are dated to between ~ 13.5 and ~15.3 cal ka BP. No tephras are recorded in the Ashenge sediments between ~15.3 cal. ka BP and the base of the core at ~17.0 cal. ka BP. Precision on the tephra ages varies within the model, from ~200 years for AST-1 and AST-2, to nearly ~1500 years for AST-9.

3.2. Geochemistry of the Ashenge tephras

The major and trace element composition of glass shards in the Ashenge tephras is given in Table 3 and shown in Fig. 4. Glass shards within the Ashenge tephras have a rhyolitic composition; containing 70.56–74.80 wt% SiO_2, 8.95–14.30 wt% Al_2O_3, 2.92–5.86 wt % FeO^T (all Fe as FeO) and 9.71–11.61 wt% ($Na_2O + K_2O$) (Fig. 4a and b). The Ashenge glass shards are peralkaline (Equation (1)) (Le Bas et al., 1986). AST-1; 2; 5; and 7 are further classified as comendites ($Al_2O_3 > 1.33(FeO^T + 4)$) (Le Maitre, 2002) whereas other Ashenge tephras are pantellerites ($Al_2O_3 < 1.33(FeO^T + 4)$).

Peralkaline

$$[Na_2O + K_2O]_{mol} > [Al_2O_3]_{mol} \quad (1)$$

Peraluminous

$$[Al_2O_3]_{mol} > [Na_2O + K_2O + CaO]_{mol} \quad (2)$$

Metaluminous

$$[Na_2O + K_2O]_{mol} < [Al_2O_3]_{mol} < [Na_2O + K_2O + CaO]_{mol} \quad (3)$$

Yttrium, Zr, La and Th behave as incompatible elements in the Ashenge glass shards; forming positive linear trends when plotted against one another (Fig. 4d, f). High Zr concentrations (Fig. 4f) are related to the high solubility of Zr in peralkaline melts (Watson, 1979; Pearce, 1990).

The Ashenge glass shards show three different Y/La and Zr/Th ratios (Fig. 4d, f) which are interpreted as representing three different groups of fractionating magma. The geochemistry of the Ashenge tephras is discussed below in terms of these compositional groups.

3.2.1. Group I Ashenge tephras: Y/La ≈0.6–0.9

Glass shards in Group 1 tephras (AST-1, 2, 7, 8 and 9) have lower Y/La ratios and lower Ba concentrations than other Ashenge tephras (Table 3, Fig. 4c and d). Glass shards in the Group I tephras also have typically lower Zr/Th ratios (≈37.0–54.3) than other Ashenge tephras (Fig. 4f).

The Group I tephras have a wide range of ages (~15.30–~0.3 cal. ka BP) and tephras of this composition are not recorded in the Ashenge sediments between ~6.2–~5.0 cal. ka BP. The younger and older Group I tephras can be distinguished between: AST-1 and

Table 2
Characteristics of tephras recorded in the Ashenge and Hayk lake sediments. Cryptotephras are indicated with an asterisk. Radiocarbon age estimates are provided as 95.4% confidence intervals. Hayk tephras which could not be geochemically analysed are identified in italics.

Tephra ID	Depth of base (cm)	Thickness (cm)	Description	Modelled age (cal. a BP)	Compositional group
Ashenge					
AST-1	12	2	discontinuous layer of grey, fine medium ash	546–321	I
AST-2	439	1	grey, fine medium ash	5041–4824	I
AST-3*	485	<1		5625–4975	II
AST-4*	527	<1		5871–5334	II
AST-5	610	2.5	diffuse layer of grey, fine ash with minor coarse ash	7155–6348	III
AST-6*	624	<1		7505–6485	II
AST-7*	635	<1		7578–6721	I
AST-8	745	1	grey, fine medium ash	14590–13582	I
AST-9*	758	<1		15332–13847	I
Hayk					
*HT-1**	66	<1		2611–1626	
HT-2	109	0.5	discontinuous grey, fine medium ash	2876–2460	I
*HT-3**	119	<1		2929–2513	
HT-4	146	0.5	discontinuous grey, fine medium ash	3635–2792	I
HT-5*	160	<1		3914–2913	II
HT-6*	169	<1		3981–3197	III
HT-7*	181	<1		4804–3835	IV
*HT-8**	200	<1		7382–5582	
HT-9*	268	<1		10514–8432	V
HT-10*	289	<1		11045–8903	V
*HT-11**	387	<1		11962–11299	
HT-12*	462	<1		12952–12027	IV

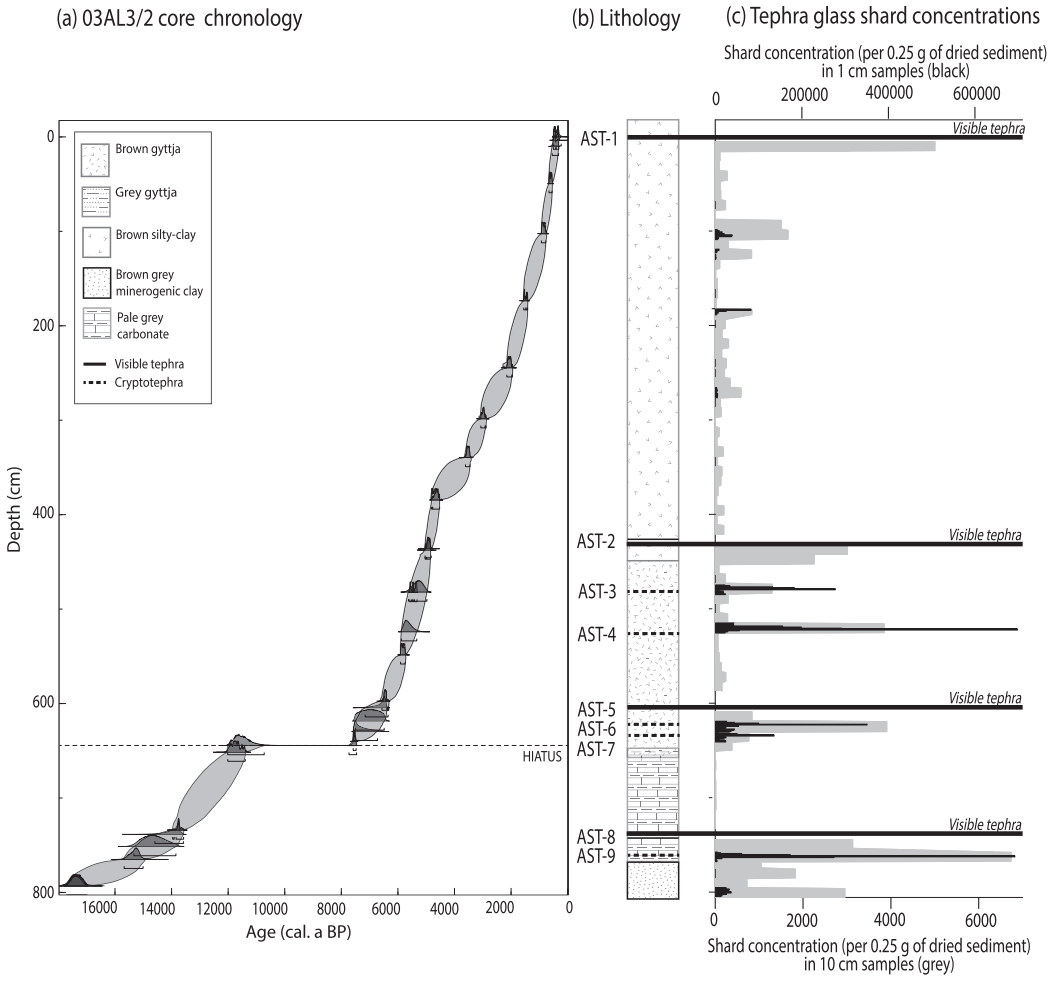

Fig. 2. (a) Ashenge 03AL3/2 lake sediment core Bayesian age model; (b) sedimentological units (Marshall et al., 2009) and visible and crypto-tephra layer occurrence, (c) cryptotephra glass shard counts throughout the Ashenge stratigraphy. Grey horizontal bars on shard concentration plots indicate shard counts (per 0.25 g of dried sediment) at 10 cm resolutions; black bars indicate concentrations in the 1 cm samples. Sampling for shard counting was not undertaken at depths where visible tephras occur.

Table 3
Normalised major element (wt%) and trace element (ppm) concentrations of glass shards in the Ashenge tephras. Average (±st. dev.) concentrations of selected elements which have proved to be useful for correlation are shown here. The range of element concentrations in each tephra is shown in italics, minimum and maximum element concentrations in glass shards from each group of tephras are given in bold. Grain specific compositions for all analytes are given in the supplementary materials.

	Group I					Group II			Group III
	AST-1	**AST-2**	**AST-7**	**AST-8**	**AST-9**	**AST-3**	**AST-4**	**AST-6**	**AST-5**
SiO_2	71.04 (0.21)	71.25 (0.37)	72.74 (0.83)	72.84 (0.17)	72.82 (0.26)	73.51 (0.29)	74.17 (0.20)	74.25 (0.28)	72.99 (0.34)
	70.71 - 71.36	***70.56*** *- 71.79*	*71.24 -* ***73.77***	*72.57-73.08*	*72.27 - 73.22*	***72.96*** *- 74.02*	*73.81 - 74.57*	*73.99 -* ***74.80***	*71.94 - 73.51*
Al_2O_3	13.58 (0.32)	13.12 (0.43)	11.45 (1.10)	10.89 (0.10)	10.63 (0.09)	10.03 (0.13)	9.33 (0.08)	9.31 (0.15)	12.85 (0.19)
	13.21 - ***14.30***	*12.66 - 13.94*	***10.08*** *- 13.40*	*10.70 - 11.05*	*10.43 - 10.78*	*9.82 -* ***10.22***	*9.20 - 9.48*	***8.95*** *- 9.47*	*12.59 - 13.31*
FeO^T	3.58 (0.21)	3.81 (0.26)	4.08 (0.57)	4.76 (0.14)	4.94 (0.14)	5.37 (0.11)	5.53 (0.53)	5.48 (0.14)	3.11 (0.14)
	3.14 *- 3.84*	*3.30 - 4.28*	*3.18 -* ***5.26***	*4.60-5.03*	*4.75-5.20*	***5.18*** *- 5.55*	*5.23 -* ***5.86***	*5.24 - 5.66*	*2.92 - 3.48*
Na_2O	6.00 (0.17)	6.04 (0.21)	6.30 (0.28)	6.07 (0.16)	6.28 (0.19)	5.82 (0.18)	5.75 (0.17)	5.81 (0.20)	5.57 (0.19)
	5.81 - 6.32	***5.59*** *- 6.47*	*5.87 -* ***7.01***	*5.89-6.35*	*5.89-6.58*	*5.43 -* ***6.26***	*5.47 - 6.07*	***5.40*** *- 6.09*	*5.09 - 6.06*
K_2O	4.80 (0.08)	4.82 (0.12)	4.77 (0.21)	4.45 (0.08)	4.60 (0.08)	4.46 (0.08)	4.42 (0.08)	4.41 (0.06)	4.64 (0.11)
	4.66 - 4.91	*4.52 - 5.00*	*4.57 -* ***5.23***	***4.28*** *- 4.56*	*4.50-4.75*	***4.32 - 4.58***	*4.32 - 4.57*	*4.36 - 4.52*	*4.48 - 4.94*
Y	99.7 (12.4)	109 (23.7)	127 (29.9)	233 (66.9)	153 (14.4)	209 (14.0)	213 (12.3)	223 (21.7)	205 (12.4)
	67.6 *- 113*	*87.8 - 199*	*68.6-170*	*148 -* ***291***	*128-187*	***192*** *- 241*	*193 - 240*	*199 -* ***262***	*186 - 247*
Zr	888 (110)	955 (199)	1240 (265)	2160 (596)	1160 (138)	1650 (107)	1660 (98.2)	1770 (177)	1480 (87.1)
	590 *- 1000*	*753 - 1730*	*681 - 1590*	*1440 -* ***2720***	*876 - 1380*	*1510 - 1860*	***1450*** *- 1860*	*1590 -* ***2080***	*1320 -1780*
Nb	160 (18.9)	172 (43.2)	207 (42.1)	366 (103)	233 (12.3)	226 (8.12)	239 (7.81)	253 (9.88)	157 (4.87)
	106 *- 169*	*141 - 353*	*106 - 256*	*235 -* ***460***	*205 - 253*	***213*** *- 240*	*224 - 257*	*240 -* ***271***	*150 - 171*
Ba	5.30 (3.10)	4.46 (2.70)	3.64 (2.54)	7.44 (3.08)	6.54 (2.27)	30.1 (6.99)	30.9 (2.88)	37.9 (4.97)	303 (24.4)
	2.01 - 10.8	*0.860 -* ***11.7***	***0.560*** *- 7.29*	*1.26 - 11.1*	*3.09 - 11.2*	*25.2 -* ***53.3***	***24.6*** *- 34.6*	*32.8 - 46.6*	*235 - 370*
La	122 (14.8)	133 (28.9)	154 (35.3)	284 (79.8)	181 (15.4)	186 (11.3)	190 (11.1)	197 (21.0)	143 (8.4)
	82.2 *- 134*	*99.7 - 242*	*83.7 - 205*	*187 -* ***356***	*152 - 206*	***171*** *- 208*	*172 - 221*	*176 -* ***246***	*127 - 170*
Ce	230 (28.2)	240 (30.1)	278 (57.2)	502 (132)	263 (25.4)	329 (16.5)	341 (14.9)	371 (25.4)	259 (13.2)
	152 - 250	*196 - 342*	***148*** *- 346*	*335 -* ***619***	*206 - 304*	***306*** *- 361*	*312 - 369*	*344 -* ***427***	*232 - 294*
Hf	22.6 (3.40)	27.3 (13.5)	31.0 (5.99)	55.7 (15.4)	35.4 (3.79)	43.6 (2.48)	43.3 (3.26)	45.3 (4.32)	40.1 (2.90)
	13.7 *- 26.4*	*19.6 -* ***83.3***	*18.1 - 39.0*	*34.3 - 72.4*	*27.5 - 40.9*	*40.0 - 47.5*	***36.0*** *- 49.3*	*40.4 -* ***53.0***	*35.2 - 48.6*
Th	19.2 (2.67)	20.7 (4.19)	24.5 (5.10)	42.5 (11.6)	25.9 (2.87)	28.7 (1.99)	28.9 (1.92)	30.6 (3.54)	24.1 (1.89)
	12.0 *- 21.5*	*15.3 - 36.8*	*13.9 - 32.5*	*27.1 -* ***53.1***	*20.0 - 30.3*	***24.8*** *- 32.2*	*25.7 - 33.5*	*27.0 -* ***37.4***	*21.2 - 30.5*
U	5.42 (0.661)	5.97 (1.22)	6.86 (1.09)	11.2 (3.18)	10.1 (1.31)	6.54 (0.353)	6.65 (0.354)	7.84 (0.241)	5.89 (0.412)
	3.58 *- 5.86*	*4.65 - 10.8*	*4.03 - 8.14*	*7.27 -* ***14.5***	*8.44 - 13.3*	***5.98*** *- 7.33*	*6.05 - 7.29*	*7.48 -* ***8.17***	*5.63 - 6.94*
	$n = 10$	$n = 20$	$n = 12$	$n = 9$	$n = 16$	$n = 14$	$n = 20$	$n = 10$	$n = 10$

AST-2, contain lower SiO_2 and FeO^T concentrations and higher Al_2O_3 concentrations than the older AST-8 and AST-9 (Table 3, Fig. 4a and b). AST-8 glass shards are compositionally bimodal; one population has a similar composition to other Group I tephras whilst those in the second population are more evolved, containing glass shards with comparatively higher Y, Zr, La and Th concentrations (Fig. 4d–f). The first tephra recorded after the hiatus in the lake record, AST-7, contains glass shards which cannot be compositionally distinguished from other Group I Ashenge tephra glass shards.

3.2.2. Group II Ashenge tephras:Y/La ≈ 1.1–1.3

Group II Ashenge tephra glass shards (AST-3, 4 and 6) are restricted to the mid-Holocene (~7.5–~4.9 cal. ka BP) sediments. Their glass shards have higher Y/La ratios and contain higher Ba concentrations than Group I tephras (Table 3, Fig. 4c and d). Group II tephra glass shards contain broadly higher Zr/Th ratios (≈42.3–61.8) when compared to Group I tephra glass shards (Fig. 4f). Glass shards in Group II tephras contain the highest SiO_2 and FeO^T and the lowest Al_2O_3 concentrations when compared with other Ashenge tephras (Table 3, Fig. 4a and b).

The Group II Ashenge tephras have differing glass shard compositions. Glass shards in AST-3 contain lower SiO_2 and higher Al_2O_3 concentrations than AST-4 and AST-6 (Table 3, Fig. 4a and b).

3.2.3. Group III Ashenge tephras: Y/La ≈ 1.4–1.5

AST-5 (~7.2–~6.3 cal. ka BP) has a distinct composition when compared with all other Ashenge tephras and is the sole member of Group III. Glass shards in AST-5 have the highest Y/La and Ba concentrations amongst the Ashenge tephras (Table 3, Fig. 4c, e). Group III tephra shards have the highest Zr/Th ratios (≈57.0–65.2) of the Ashenge tephras. Plots of SiO_2 against Al_2O_3 and FeO^T (Fig. 4a and b) concentrations in the Ashenge glass shards show that AST-5 glass shards have distinct major element ratios when compared with other Ashenge glass shards.

3.3. Tephrochronology of the Hayk sediments

The Hayk sediments contain a total of 12 tephras, ranging in age from ~13.0 to ~1.6 cal. ka BP. HT-2 and HT-4 are visible tephras, comprised of well sorted, grey-white coloured fine to medium grained ash and occur as 0.5–1 cm thick discontinuous layers in the core (Table 2). Ten cryptotephras were identified through glass shard counting (Fig. 3). Unfortunately, due to heavy sampling of the core after cryptotephra processing, more material from HT-1, HT-3, HT-8 and HT-11 could not be sampled for geochemical analysis.

Historical tephra layers are not recorded in the Hayk sediments, the youngest tephra (HT-1) dating to ~2.6–~1.6 cal. ka BP. Tephras are also not recorded in the sediments beneath the oldest tephra (12.9–12.0 cal. ka BP) and the base of the core at 16.0 cal ka BP. Precision on the ages of these tephras varies within the age model, ranging from ~400 years for HT-2 and HT-3 to ~2000 years for HT-8; 9 and HT-10, at the 95.4% confidence level.

3.4. Geochemistry of the Hayk tephras

The major and trace element composition of the Hayk tephra glass shards is given in Table 4 and shown in Fig. 5. The Hayk glass

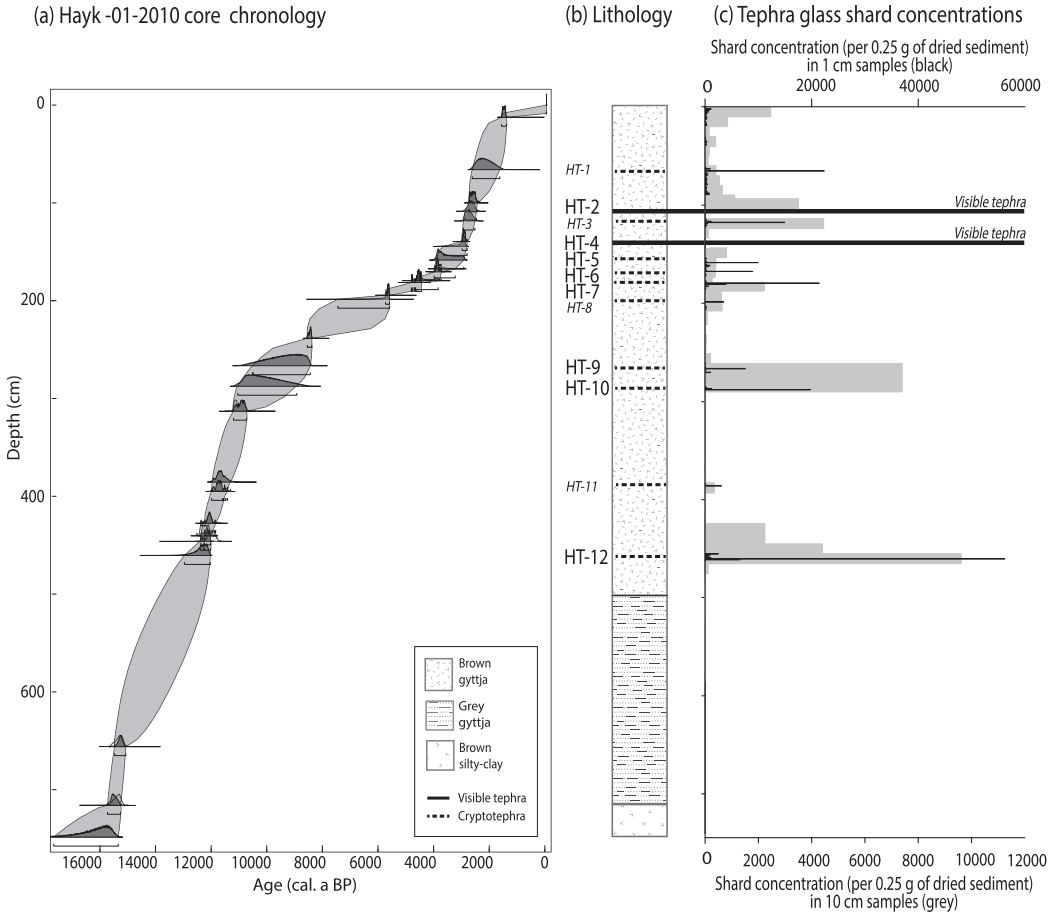

Fig. 3. (a) Hayk-01-2010 lake sediment core Bayesian age model; (b) sedimentological units and visible and crypto-tephra layer occurrence, tephras not analysed are labelled in italics, (c) cryptotephra glass shard counts throughout the Hayk stratigraphy. Grey horizontal bars on shard concentration plots indicate shard counts (per 0.25 g of dried sediment) at 10 cm resolutions; black bars indicate concentrations in the 1 cm samples. Sampling for shard counting was not undertaken at depths where visible tephras occur.

shards have a rhyolitic composition; containing 72.78–75.41 wt% SiO_2, 9.73–14.39 wt% Al_2O_3, 1.48–5.44 wt% FeO^T, 7.63–10.36 wt% ($Na_2O + K_2O$) (Fig. 5). The majority of Hayk glass shards have a peralkaline affinity, however, HT-2 and HT-4 are marginally metaluminous (Equation (3)) and HT-5 and HT-6 are marginally peraluminous (Equation (2)) (Le Bas et al., 1986). HT-7 and HT-12 can be further classified as comendites and HT-9 and HT-10 as pantellerites (Le Maitre, 2002).

Yttrium, Zr, La and Th form positive linear arrays when plotted against one another; indicating they are all incompatible in the Hayk glass shards. Glass shards in the Hayk tephras show curvilinear Y/Nb positive trends; indicating that Nb becomes compatible at the onset of a new mineral phase crystallising, whilst Y remains incompatible. The Hayk tephras can be divided into five groups based on the Zr/Th and Y/La ratios of their glass shards (Fig. 5f), the composition of these tephras is discussed below in relation to these groups.

3.4.1. Group I Hayk tephras: Zr/Th ≈30.4–37.9

Glass shards in Group I tephras (HT-2 and HT-4) are the youngest tephras (~3.6–~2.5 cal. ka BP) in the Hayk core to have been analysed and have the differing Zr/Th ratios to older Hayk glass shards.

Group I tephra glass shards contain lower FeO^T concentrations than Hayk Group IV and higher FeO^T concentrations than Hayk Group II, III and V glass shards. Glass shards in the Group I tephras are depleted in Y, Nb, La and Th relative to glass shards in all other Hayk tephras. Glass shards in Group I tephras contain higher Ba concentrations than Group IV and V glass shards and lower Ba concentrations than Group II and III tephra glass shards.

HT-2 and HT-4 tephras cannot be distinguished compositionally; although HT-2 glass shards contain broadly higher Y concentrations than HT-4.

3.4.2. Group II Hayk tephras: Zr/Th ≈18.9–23.2

The late-Holocene HT-5 (~3.9–~2.9 cal. ka BP) is the sole tephra member of Group II, with a distinct Zr/Th ratio to glass shards in other Hayk tephras. Glass shards in this tephra are distinguished from other Hayk tephras on the basis of their higher Ba concentrations. HT-5 and HT-6 glass shards have broadly lower Y/La ratios (≈0.8–0.9) when compared with other Hayk tephras (≈0.9–1.2). However, HT-5 contains higher Y, Zr, La and Ba concentrations than HT-6 glass shards.

3.4.3. Group III Hayk tephras: Zr/Th ≈15.1–16.9

HT-6 (3.9–3.2 cal. ka BP) is the only tephra in Group III; its glass shards contain distinctly lower Zr concentrations than all other Hayk tephras.

3.4.4. Group IV Hayk tephras: Zr/Th ≈55.1–65.7

Group IV Hayk tephras (HT-7 and HT-12) are easily distinguished from other Hayk tephras, containing higher FeO^T and Zr

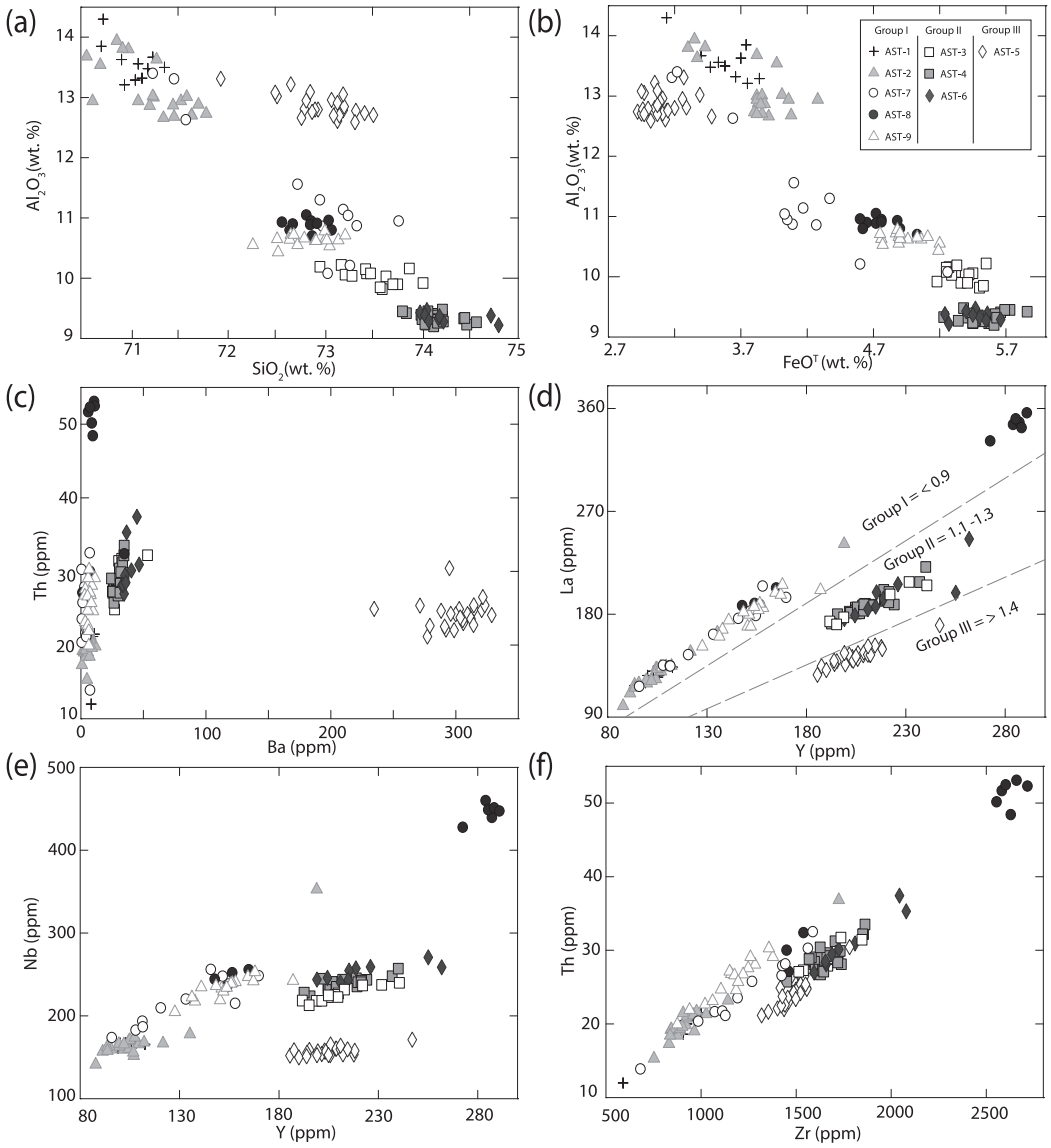

Fig. 4. Major and trace element composition of single shards from the Ashenge tephras. Incompatible element ratios (d and e) divide the Ashenge tephras into three compositional groups.

and lower Al_2O_3 than other Hayk tephras (Table 4, Fig. 5b, f). Group IV tephras have the widest ranges of ages (~13.0–~3.8 cal. ka BP) when compared with all other tephra groups recorded in the Hayk sediments.

HT-7 contains higher Zr, La and Th and lower Al_2O_3 and Ba when compared with glass shards in HT-12, the oldest tephra identified in the Hayk sediments (Fig. 5a, d, f).

3.4.5. *Group V Hayk tephras: Zr/Th ≈11.5–14.2*

Group V tephras (HT-9 and HT-10) are restricted to the early Holocene (~11.0–~8.4 cal. a BP) section of the Hayk sediments. Their glass shards have distinct Zr/Th ratios when compared with other Hayk tephra glass shards (Table 4, Fig. 5f). Glass shards in these tephras are more enriched in Th when compared with other Hayk tephras (Fig. 5f).

Glass shards in HT-9 contain higher Zr, Nb, La and Th compared to glass shards in HT-10 (Fig. 5c–f).

4. Discussion

4.1. *Tephra correlations between lakes Ashenge and Hayk*

The major and trace element composition of the Ashenge and Hayk tephra glass shards is compared in Figs. 6 and 7 to test whether there are potential tephra correlations between the archives. For the majority of tephra deposits in the Ashenge and Hayk cores, the major and trace element compositions of their component glass shards are distinct. Nonetheless, some tephra deposits within both lakes have compositionally similar glass shards.

Hayk Group IV tephras (HT-7 and HT-12) have similar Y/La (≈1.0–1.1) and Zr/Th (≈55.1–65.7) ratios to Ashenge Group II (Y/La ≈1.1–1.3, Zr/Th ≈53.5–61.8) tephras (AST-3, AST-4 and AST-6) (Fig. 6). Bi-plots of the first three principal components from Principal Component Analysis of Y, Zr, Nb, Ba, La and Th concentrations in the Ashenge and Hayk tephra glass shards are shown in Fig. 10. This demonstrates that there are statistical similarities

Table 4
Average normalised major element (wt%) and trace element (ppm) concentrations of glass shards in each of the Hayk tephras. Selected elements which have proved to be useful for correlation are shown here. The standard deviation the concentration of each element in each tephra is given in brackets, the range of element concentrations in each tephra is given in italics. Major element concentrations are presented to two decimal places and trace element concentrations are presented to three significant figures, the grain specific compositions for all analytes are given in the supplementary materials.

	Group I		Group II	Group III	Group IV		Group V	
	HT-2	**HT-4**	**HT-5**	**HT-6**	**HT-7**	**HT-12**	**HT-9**	**HT-10**
SiO_2	73.26 (0.17)	73.45 (0.37)	74.31 (0.40)	74.18 (0.27)	73.78 (0.15)	73.44 (0.24)	74.23 (0.37)	73.71 (0.22)
	*73.07 - **75.53***	***72.88** - 74.48*	*73.65 - 75.18*	*73.87 - 74.57*	*73.48 - **74.02***	***72.78** - 73.82*	*73.87 - **75.41***	***73.33** - 74.19*
Al_2O_3	13.28 (0.14)	13.21 (0.18)	13.66 (0.11)	14.03 (0.32)	9.81 (0.05)	10.33 (0.09)	12.98 (0.12)	13.48 (0.21)
	13.14 - 13.52	***12.75 - 13.66***	*13.46 - 13.84*	*13.44 - 14.39*	***9.73** - 9.91*	*10.11 - **10.52***	***12.82** - 13.33*	*13.17 - **13.95***
FeO^T	2.92 (0.13)	2.85 (0.13)	1.88 (0.20)	1.72 (0.15)	5.28 (0.11)	5.13 (0.14)	2.02 (0.08)	2.01 (0.10)
	*2.69 - **3.18***	***2.50** - 3.12*	*1.50 - 2.38*	*1.48 - 1.89*	*5.07 - 5.44*	***4.89 - 5.44***	*1.90 - 2.21*	***1.81** - 2.18*
Na_2O	4.90 (0.17)	4.79 (0.15)	4.34 (0.39)	4.31 (0.12)	5.53 (0.15)	5.46 (0.14)	4.86 (0.41)	4.77 (0.12)
	*4.54 - **5.12***	***4.45** - 5.05*	*3.30 - 4.70*	*4.14 - 4.47*	*5.28 - **5.84***	***5.19** - 5.81*	***3.58 - 5.27***	*4.57 - 4.94*
K_2O	3.64 (0.07)	3.73 (0.10)	4.39 (0.08)	4.47 (0.04)	4.46 (0.07)	4.54 (0.08)	4.81 (0.10)	4.86 (0.07)
	***3.52** - 3.72*	*3.58 - **4.00***	*4.27 - 4.55*	*4.44 - 4.55*	***4.35** - 4.56*	*4.37 - **4.67***	***4.69 - 5.04***	*4.73 - 5.00*
Y	82.4 (5.08)	71.9 (6.20)	109 (8.59)	87.2 (3.57)	245 (16.7)	191 (9.16)	163 (18.7)	122 (14.6)
	*74.3 - **91.3***	***59.3** - 80.5*	*92.8 -118*	*80.9 - 92.1*	*215 - **289***	***170** - 202*	*118 - **198***	***100** - 149*
Zr	609 (31.4)	553 (51.1)	616 (38.9)	401 (14.2)	1870 (127.7)	1560 (90.1)	772 (78.4)	613 (68.6)
	*570 - **670***	***471** - 638*	*528 - 679*	*377 - 425*	*1670 - **2190***	***1330** - 1660*	*576 - **879***	***505** - 739*
Nb	73.8 (2.50)	71.3 (4.37)	103 (3.04)	101 (5.58)	249 (7.86)	220 (5.09)	277 (17.7)	248 (15.5)
	70.5 - 77.7	***65.4 - 81.6***	*95.3 -107*	*92.0 - 109*	*238 - **268***	***210** - 229*	*237 - **307***	***225** - 274*
Ba	733 (37.0)	680 (42.0)	1210 (70.4)	1000 (44.6)	37.6 (10.6)	108 (5.96)	25.0 (10.4)	23.1 (12.7)
	*677 - **805***	***609** - 757*	*1070 - 1320*	*935 - 1050*	***25.2** - 74.8*	*95.6 - **116***	***4.51** - 45.3*	*9.12 - **60.6***
La	82.1 (4.34)	73.2 (6.80)	123 (10.3)	109 (5.42)	224 (16.7)	175 (9.68)	148 (16.7)	115 (9.29)
	*76.9 - **90.6***	***62.7** - 83.0*	*98.5 - 134*	*100 - 115*	*199 - **267***	***153** - 188*	*111 - **181***	***99.5** - 133*
Ce	153 (4.61)	146 (8.58)	213 (16.6)	187 (7.72)	391 (22.9)	349 (15.5)	283 (20.2)	228 (21.6)
	*148 - **164***	***130** - 159*	*175 - 232*	*171 - 195*	*356 - **458***	***309** - 374*	*229 - **321***	***197** - 280*
Hf	17.2 (1.67)	16.1 (1.70)	19.9 (2.05)	13.7 (0.972)	47.0 (3.61)	40.4 (2.09)	30.0 (3.66)	22.9 (2.55)
	*14.3 - **19.9***	***13.3** - 18.8*	*16.4 - 23.7*	*12.3 - 14.8*	*40.4 - **54.3***	***35.6** - 43.0*	*22.2 - **37.1***	***17.2** - 27.0*
Th	17.8 (1.12)	16.7 (1.70)	29.9 (1.96)	25.7 (1.58)	31.2 (1.81)	26.6 (1.40)	59.9 (6.66)	47.2 (3.94)
	*16.1 - **19.6***	***13.9** - 18.9*	*26.0 - 32.5*	*25.7 - 27.6*	*28.0 - **35.5***	***23.0** - 28.3*	*46.0 - **70.4***	***41.9** - 55.4*
U	4.41 (0.311)	4.59 (0.351)	6.08 (0.453)	5.62 (0.382)	7.01 (0.343)	7.40 (0.252)	16.1 (0.913)	15.9 (1.06)
	***3.89** - 4.90*	*3.98 - **5.28***	*5.01 - 6.71*	*4.85 - 5.97*	***6.44 - 7.81***	*7.00 - 7.74*	*15.1 - **18.4***	***14.2** - 17.7*
	$n = 12$	$n = 19$	$n = 15$	$n = 8$	$n = 20$	$n = 18$	$n = 15$	$n = 12$

between the compositions of the Ashenge Group II and Hayk Group IV glass shards.

HT-7 glass shards are compositionally similar to AST-3 (Fig. 7). However, HT-7 is also more compositionally evolved than AST-3, containing higher concentrations of SiO_2 and incompatible trace elements and lower concentrations of Al_2O_3 than AST-3. Furthermore, HT-7 (~4.8–~3.8 cal. ka BP) is too young to correlate with AST-3 (~5.6–~4.9 cal. ka BP). This is consistent with HT-7 and AST-3 being produced by two separate eruptions from the same source, with a time interval between allowing fractional crystallisation of feldspar and ilmenite from the source magma chamber and the subsequent eruption of the more evolved HT-7. Glass shards in HT-12 (Hayk Group IV) have similar incompatible element ratios to the Ashenge Group II tephras. However glass shards in HT-12 are enriched in Ba (Fig. 6c) relative to AST-3, 4 and 6 and HT-12 is too old (12.9–12.0 cal. ka BP) to correlate with the Ashenge Group II tephras.

It is apparent that the lake Ashenge and Hayk sediments record different eruptive events, however, glass shards in Ashenge Group II and Hayk Group IV tephras have similar incompatible element ratios, suggesting they may be derived from the same source. Furthermore, the new age models presented in this study reveals that, of the 9 tephra layers in Lake Ashenge and 12 in Lake Hayk, there is very little temporal overlap. Tephra HT-8, dated to ~7.8–~5.5 cal. ka BP, shows the only possible chronological correlation, overlapping within 95.4% confidence intervals with tephra layers AST-4, 5, 6, and 7 (~6.7–~5.9 cal. ka BP). Unfortunately, HT-8 could not be analysed, so the potential for correlation here cannot be tested. A number of samples between 110–290 cm depth in the Ashenge archive revealed tephra glass shards at lower concentrations (<100,000 shards per 0.25 g of dried sediment) which were not investigated in this study. Such cryptotephra, if they can be resolved and analysed, could potentially provide correlative layers to HT-1 to HT-7 which date from the same time period. Further work is, however, needed to investigate cryptotephras associated with low shard concentrations throughout the Ashenge archive, and this may reveal further correlations.

A sedimentary hiatus within the Ashenge stratigraphy, associated with an early Holocene lowstand, spans ~11.8 to 7.6 cal ka BP (Marshall et al., 2009). During this lowstand, tephras deposited at Lake Ashenge may have been eroded or reworked, and this may limit the potential for correlation to HT-9 and HT-10 (11.0–8.4 cal. ka BP).

The lack of correlations between archives collected from lakes <140 km apart in the Ethiopian Highlands may be related to additional factors. Lake Hayk is located in a sheltered setting, separated from the Afar Triangle to the east by a series of horsts attaining <2400 m height. Lake Ashenge is located <10 km from the rift margin and the elevation to the east drops rapidly into the Afar Triangle. Therefore, Lake Ashenge is more exposed to the Afar

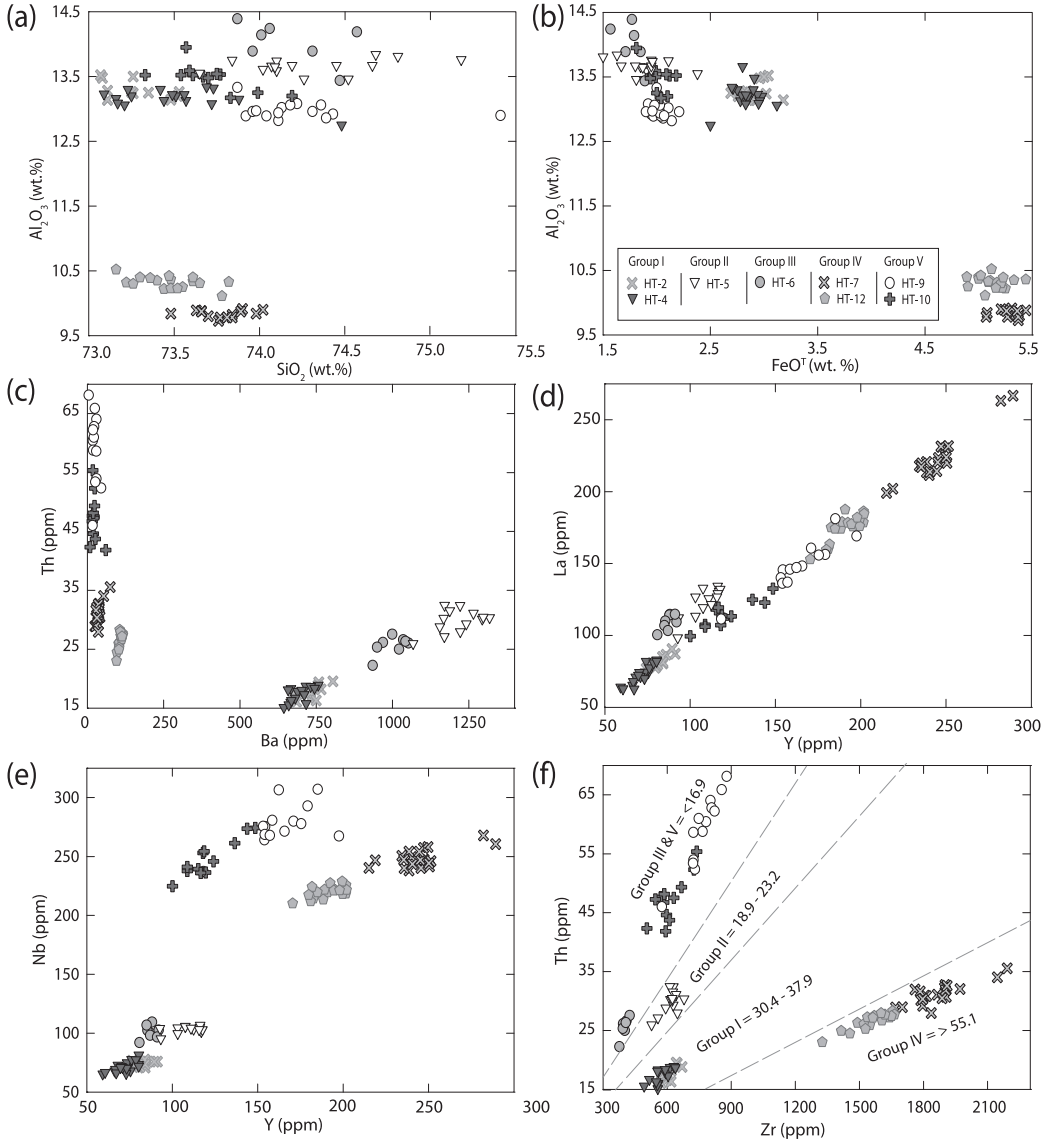

Fig. 5. Glass compositions of the Hayk tephras. (a) and (b) HT-10 and HT-12 contain lower Al_2O_3 and higher FeO^T concentrations than other Hayk tephras, (f) the Hayk tephra glass shards have five different Zr/Th ratios.

Triangle and more likely to receive tephra deposits; particularly if the eruptions are localised. Lake Ashenge is located to the north of Lake Hayk and this may determine the type and frequency of tephras received; eruptions from the northern Afar may be supplying the tephras in Lake Ashenge, whilst the tephras recorded in Lake Hayk be derived from the southern Afar. To deposit a tephra from the same event in these different lakes, a change in wind-direction during the eruption may be required (see Fig. 1). Lakes Ashenge and Hayk are alkaline lakes (pH ~8.8–9) (Lamb et al., 2007; Marshall et al., 2009). Rhyolitic glass is more soluble in alkali conditions (Mariner and Surdam, 1970) and variations in lake alkalinity through time may therefore determine the preservation of glass shards in the archives. Tephra glass shards observed in the Ashenge and Hayk archives are pristine, however, variable glass preservation could be responsible for the lack of correlations.

4.2. Eruption tempo and characteristics

The distribution of visible and crypto-tephras in the Ashenge and Hayk stratigraphies gives an insight into the frequency of past eruptions. Despite the limitations associated with taphonomic processes at lakes Ashenge and Hayk, this work presents the most comprehensive information on past eruption frequency for this region so far available.

Table 2 shows Bayesian modelled ages of the tephras recorded in the Ashenge and Hayk archives. Thirteen of the total 21 tephras documented in both archives occur at ~7.5–~1.6 cal. ka BP; potentially reflecting a peak in explosive volcanism during this period. Tephras are recorded frequently in both archives between ~15.3–~1.6 cal. ka BP, indicating explosive eruptions in this area occurred at an average of every ~1000 years during this period. The only recent tephra recorded over the past 1.6 cal ka BP is the ~0.5–~0.3 cal. ka BP AST-1, in the Ashenge core.

Selected compositional parameters (major and trace element concentrations and incompatible element ratios) from glass shards in separate tephra groups are plotted against their age in Fig. 8. Glass shards from each individual tephra in lakes Ashenge and Hayk occupy a wide compositional range. This compositional

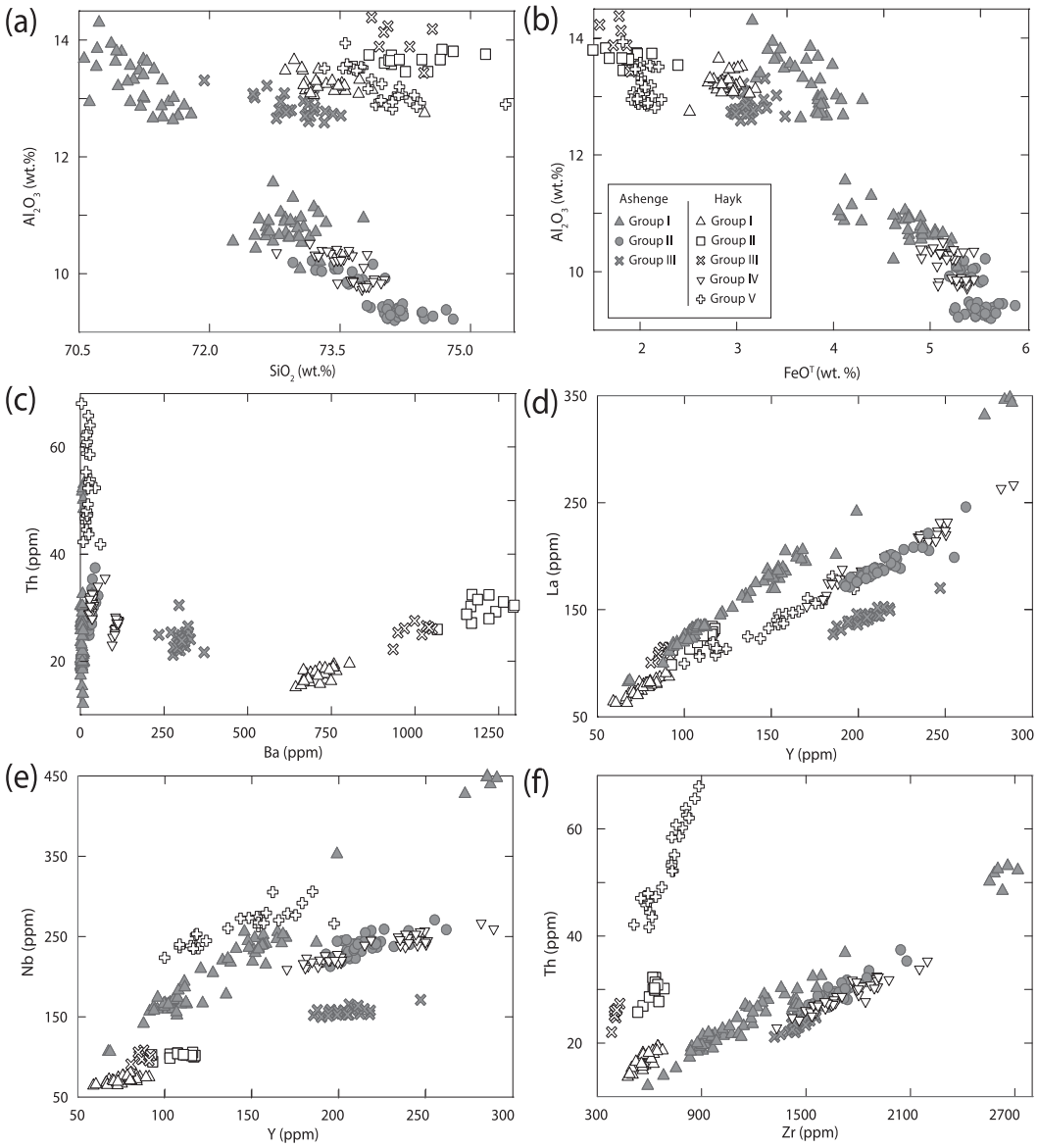

Fig. 6. Major and trace element bi-plots comparing the composition of the Ashenge and Hayk tephras.

heterogeneity suggests that these tephras are derived from evolving or compositionally zoned magma chambers.

The Ashenge Group I tephras have a wider range of ages (~15.3–~0.3 cal. ka BP) than other tephra compositional groups recorded in the archives. The Ashenge Group I tephras may represent intermittent eruptions from a distant caldera active over a long time period. A lack of documented Ashenge Group I tephras at ~16.7–~13.6 cal. ka BP and ~4.8–~0.3 cal. ka BP and are potentially associated with periods of repose.

Whilst the similar incompatible element ratios of the Ashenge Group I tephras suggests these tephras have a co-magmatic origin, their tephra glass shards become depleted in SiO_2, FeO^T and Y and enriched in Al_2O_3 concentrations through time. This trend is the opposite to that which would be expected for simple crystal fractionation of a feldspar dominated assemblage. To constrain the petrogenesis of the tephras, detailed mapping and sampling of the potential source volcanoes is required. However, it is apparent that other processes (possibly recharge and/or assimilation) are involved in their petrogenesis.

Other compositional groups (e.g. Hayk Group I and V) recorded in the archives are comprised of eruptions covering relatively short times spans (<~3 ka). These tephras are more chemically homogeneous than eruptions depositing the Ashenge Group I tephras, this may be an indication of compositional zoning developing in the magma chambers with relatively longer repose periods. However, the Hayk Group I and V tephra glass shards show enrichment in Y through time when compared to older tephras from the same compositional group. This indicates that the evolution of the Hayk tephras was dominated by fractional crystallisation of feldspar, differing to the Ashenge Group I melt evolution.

4.3. Provenance of the lakes Ashenge and Hayk tephras

The closest volcanoes to lakes Ashenge and Hayk that are thought to have been active during the Holocene are located to the east in the Afar Triangle (Siebert et al., 2011, Fig. 1). Given the lack of

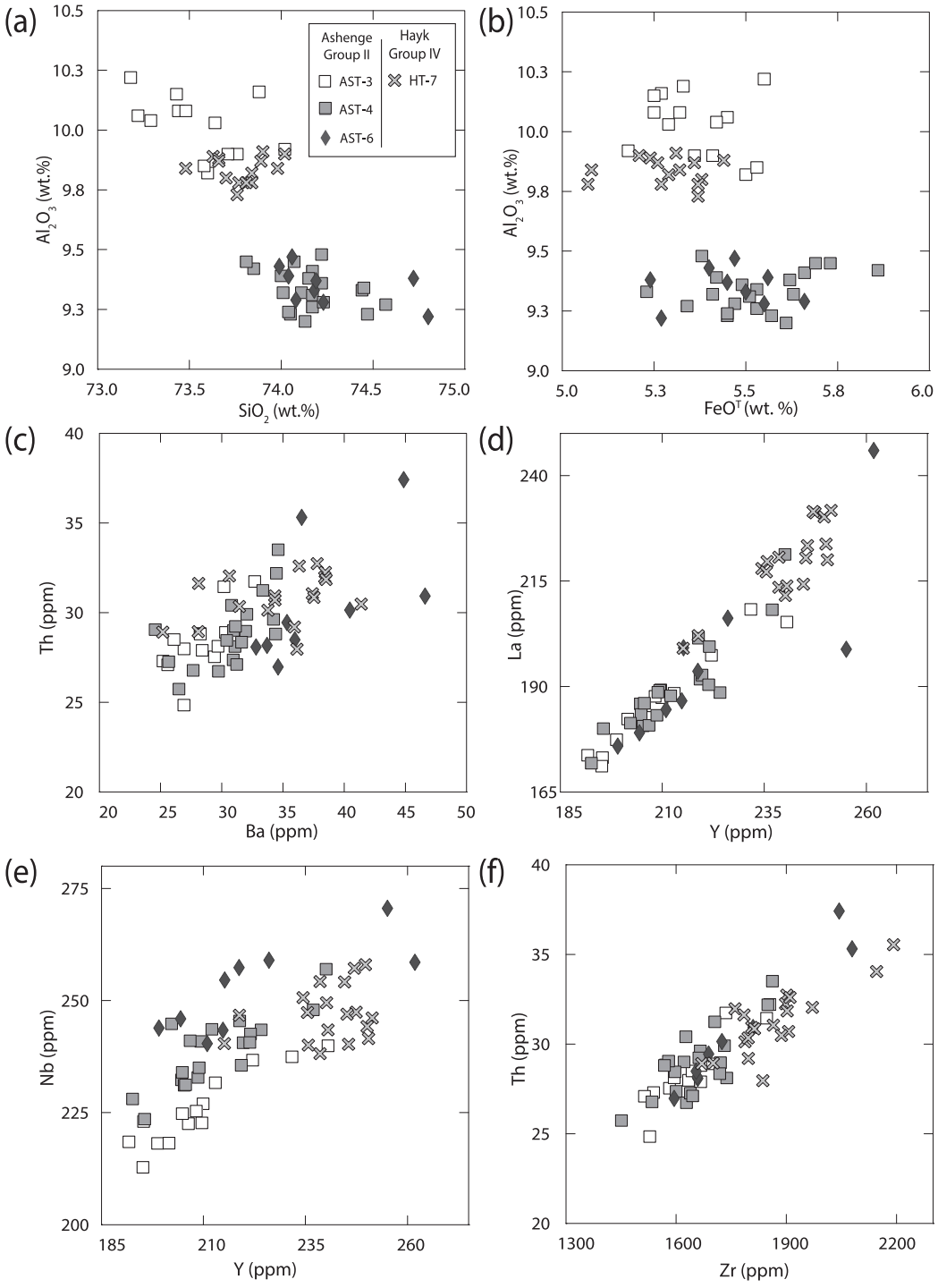

Fig. 7. Major and trace element bi-plots comparing the composition of HT-7 with Ashenge Group 2 tephras: AST-3; 4; 6. HT-7 has a similar, but more evolved composition than AST-3, containing higher Y, Nb, Zr, SiO_2 and lower Al_2O_3.

correlations between lakes Ashenge and Hayk, it is likely that the tephras recorded in these archives are locally derived.

There is a scarcity of geochemical and chronological data from Holocene volcanic deposits in the Afar Triangle. Therefore, it is currently not possible to assess correlations with all possible source volcanoes which could have generated tephras deposited in lakes Ashenge and Hayk during the Holocene. The Ashenge and Hayk tephras are compared here with published glass analyses on proximal pumice and obsidians from Dabbahu volcano and new glass analyses on proximal tephra deposits from the Dubbi volcano (Eritrea).

Dabbahu (Boina) (Fig. 1) is the closest volcano to lakes Ashenge and Hayk with published geochemical data. Glass analyses of proximal pumice and obsidian samples from Dabbahu (Field et al., 2012) are compared with Ashenge and Hayk tephra glass shard analyses in Fig. 9. Dabbahu glass contains similar Y/La ratios

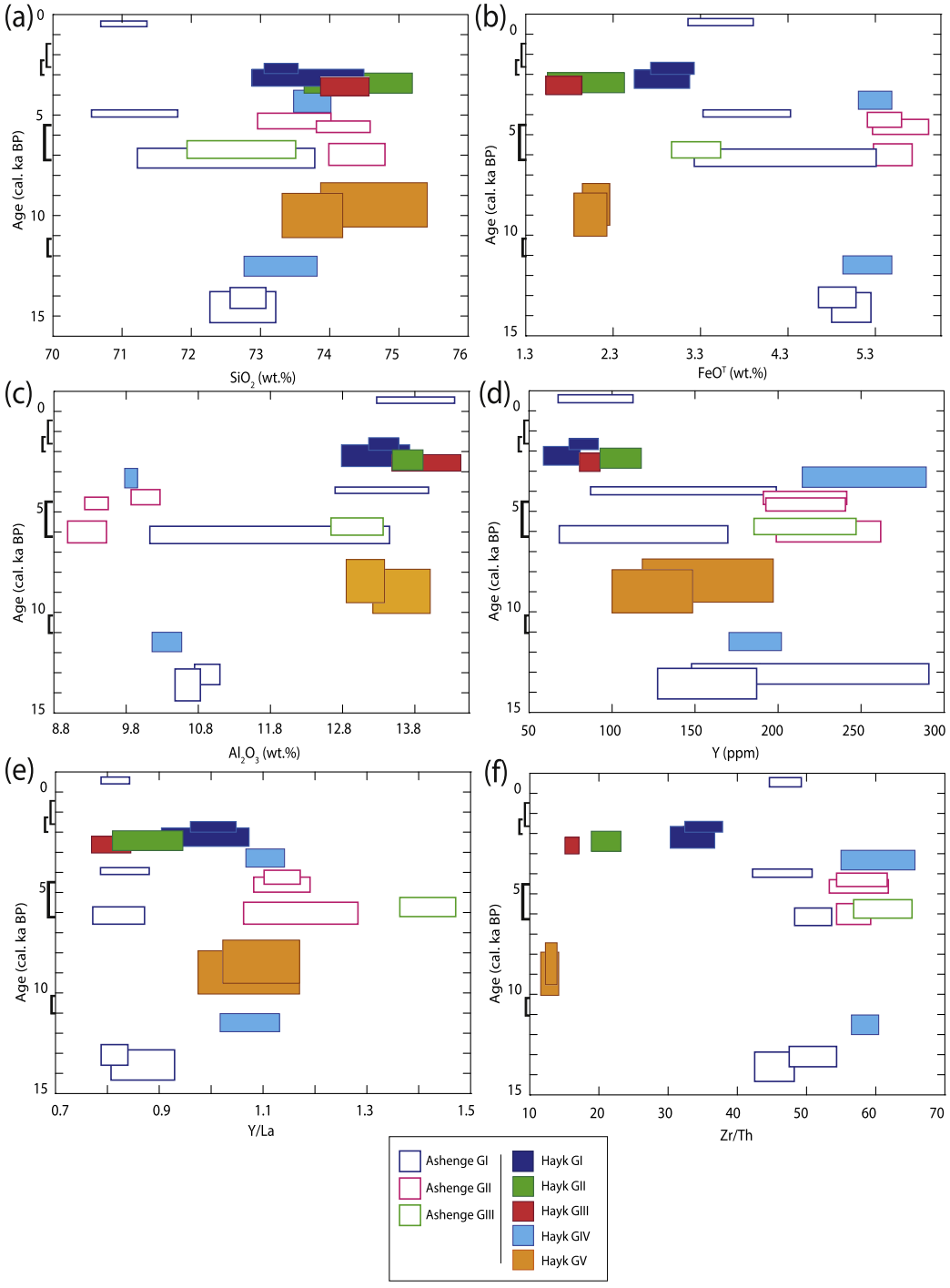

Fig. 8. Major and trace element concentrations and incompatible element ratios of glass shards in the Ashenge and Hayk tephras plotted against their modelled tephra age. Brackets on the age axis indicate the age ranges of tephras that were not analysed.

(≈0.95) to some of the Hayk Group I, IV and V tephra glass shards (≈0.9–1.2). However, Dabbahu glass contains higher Zr/Th ratios (>98.8) than the Ashenge and Hayk tephra glass shards (<65.7).

Fig. 10 shows the bi-plots of the first three principal components from a PCA comparing the composition of the Ashenge and Hayk tephras with obsidian and pumice samples from Dabbahu. It is apparent that the Ashenge and Hayk tephras are statistically different to the Dabbahu obsidian and pumice. Therefore further sampling and'side-by-side' analyses of glass from Dabbahu proximal deposits are required to assess the similarity of the incompatible element ratios to some of the Hayk tephras.

The uppermost tephra in the Ashenge archive (AST-1, 546–321 cal. a BP) is the only historical tephra documented in the Ashenge and Hayk records. The AD 1861 eruption of Dubbi (270 km NE of Ashenge) dispersed volcanic ash ~300 km to the west on the Ethiopian Plateau (Wiart and Oppenheimer, 2000). A previous

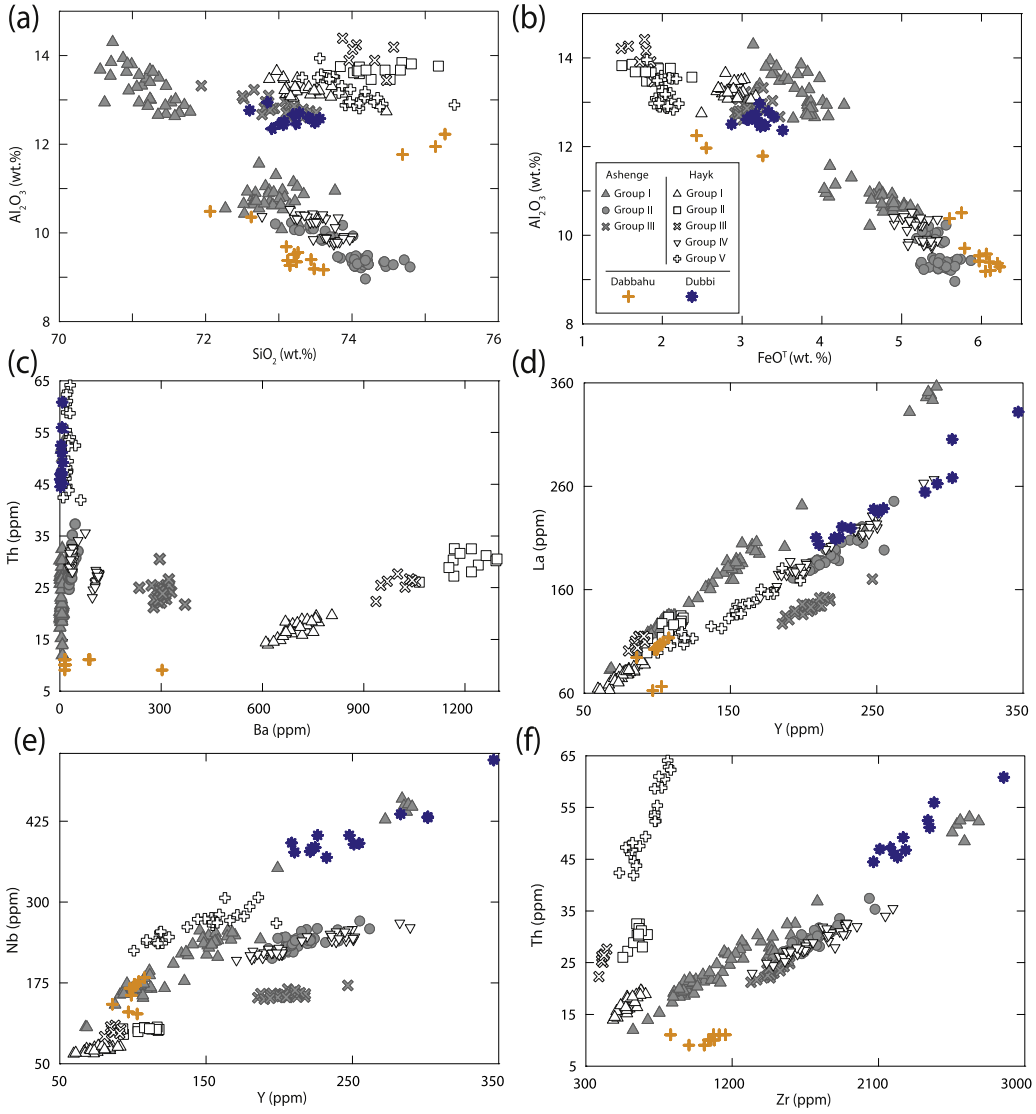

Fig. 9. Comparison of the composition of Ashenge and Hayk tephras with proximal tephra samples from the Dabbahu and Dubbi volcanoes in the Afar. Glass analyses on pumice and obsidian from Dabbahu are from Field et al. (2012), Dubbi proximal samples (from the AD, 1861 eruption) were analysed as part of this study.

eruption (VEI = 2) from Dubbi is believed to occurred in AD 1400 (Gouin, 1979) and this has a comparable age to the modelled date of AD 1404–1629 for AST-1.

Analyses of tephra glass shards from the Dubbi AD 1861 pyroclastic flow deposits are compared with the composition of AST-1 glass shards in Fig. 9 to test whether AST-1 was deposited by a possible older eruption from Dubbi (Fig. 9). The AST-1 tephra glass shards have similar Zr/Th ratios (≈44.6–49.2) to the Dubbi glass shards (≈43.3–52.3). However, AST-1 glass shards contain lower Al_2O_3 and incompatible element concentrations and higher FeO^T concentrations than the Dubbi AD 1861 tephra glass shards (Fig. 9). Further glass analysis of a wider range of proximal samples from Dubbi is therefore required to investigate the source of AST-1.

5. Conclusions

Distal tephras in lake sediment archives from the Ethiopian Highlands provide a <17 cal. ka BP record of peralkaline volcanism from the Afar Triangle. Here we present an initial late Pleistocene to Holocene tephra framework for the Afar region, the first to cover this temporal and spatial range. This is the first instance where cryptotephras have been identified and dated in terrestrial archives from Ethiopia; of the 21 tephra layers across the two study sites, 15 of these were identified as cryptotephra layers. These results highlight the essential contribution of cryptotephra studies to our understanding of past volcanism. Furthermore, this study provides the first database of shard-specific major and trace element compositions for tephras from Ethiopia over this temporal range.

Lakes Ashenge and Hayk record different eruptive events. The lack of correlations between archives collected from <140 km apart may be associated with numerous factors. The taphonomic and preservation issues at Ashenge and Hayk highlight the importance of compiling data from multiple sediment archives in order to provide more complete records of volcanic activity through time.

Nonetheless, the Ashenge and Hayk archives provide a valuable insight into the regional eruption history. This tephra record demonstrates that potentially seven volcanic centres in the Afar have erupted frequently and explosively over the past <15 cal. ka

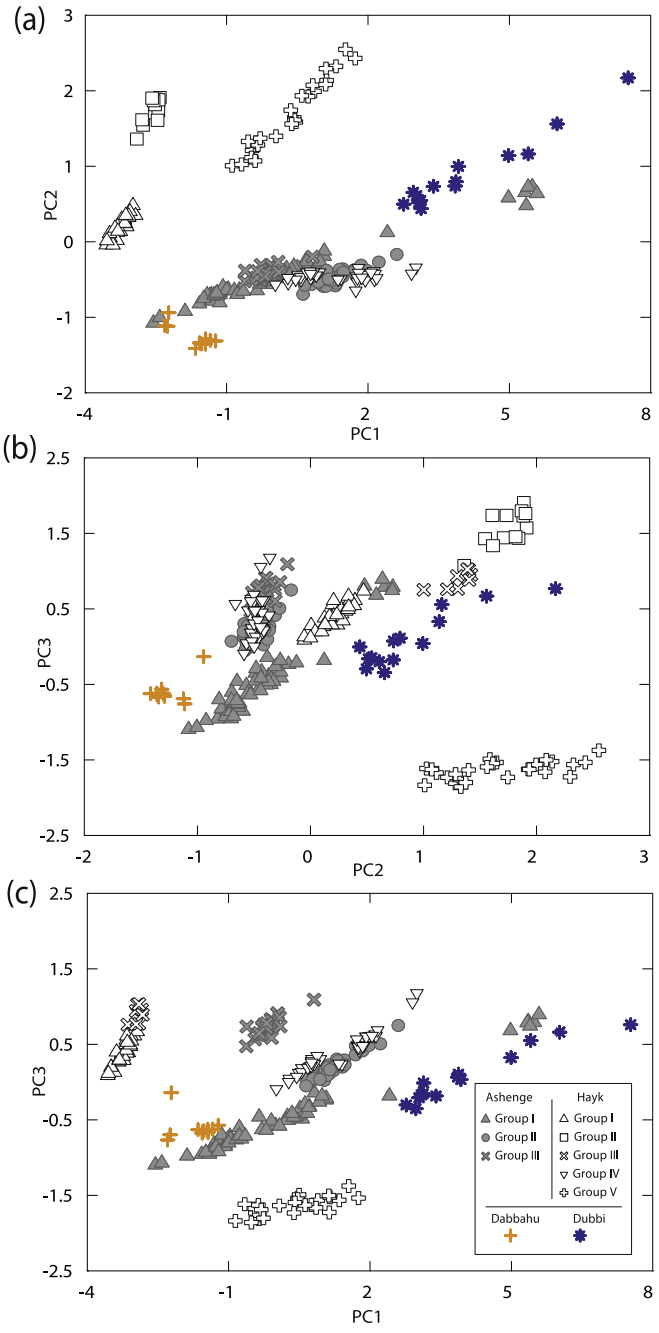

Fig. 10. Bi-plots of the first three Principal Components from Principal Component Analysis of Y, Zr, Nb, Ba, La and Th concentrations of tephras from Ashenge, Hayk, Dabbahu and Dubbi.

BP; with the majority of tephras recorded at ~7.5–~1.6 cal. ka BP. The only historically documented tephra layer recorded in the archives occurs at ~0.5–~0.3 cal. ka BP. Our new tephra framework provides an insight into the volcanic history of the Afar that has important implications for hazard assessments in a region where the record of recent volcanism has remained largely undocumented. The cryptotephra study focused on the identification of silica-rich tephra units, however, basaltic volcanism is common in the area and future studies may be able to build basaltic units into this initial tephra framework.

Lake sediments have been shown to provide an accessible record of past volcanism from the remote Afar Triangle. A greater network of sites must now be studied, which would capture not only the eruption frequency, but also the patterns of dispersal. This approach is, however, challenged by the lack of published major and trace element analyses of tephra glass shards from outcrops proximal to volcanoes in the Afar Triangle. Further geochemical characterisation of the regional volcanoes is therefore essential to identify the sources of tephras recorded in the lakes Ashenge and Hayk sediments as well as those that will be uncovered in future studies.

Acknowledgements

CMJ was in the receipt of a NERC (PhD grant number: 10983-01, NERC 2012) algorithm fellowship. Fieldwork at Lake Hayk was funded by the German Research Foundation within the scope of the CRC 806 (Our way to Europe). Analytical costs were supported by the LacCore Visiting Graduate Student Travel Grant Program (University of Minnesota). Katie Loakes (Loughborough University) and Helene Ducrotoy (Aberystwyth University) are thanked for providing unpublished AMS dates for the archives. The authors would like to thank the OxCal Google Group Community and Christopher Bronk Ramsey for helpful advice on age modelling.

Appendix A. Supplementary data

Supplementary data related to this article can be found at http://dx.doi.org/10.1016/j.quageo.2016.10.001.

References

Ayele, A., Kassim, M., Kidane, T., Omar, A., Tait, S., Nercessian, A., de Chabalier, J.-B., King, G., 2007a. The volcano-seismic crisis in Afar, Ethiopia, starting September 2005. Earth Planet. Sci. Lett. 255, 177–187. http://dx.doi.org/10.1016/j.epsl.2006.12.014.

Ayele, A., Stuart, G., Bastow, I.D., Keir, D., 2007b. The August 2002 earthquake sequence in north Afar: insights into the neotectonics of the Danakil microplate. J. Afr. Earth Sci. 48, 70–79. http://dx.doi.org/10.1016/j.jafrearsci.2006.06.011.

Barberi, F., Ferrara, C., Santacroce, R., Treuil, M., Varet, J., 1975. A Transitional basalt-pantellerite sequence of fractional crystallisation, the Boina Centre (Afar Rift, Ethiopia). J. Petrol. 16 (1), 22–56. http://dx.doi.org/10.1093/petrology/16.1.22.

Le Bas, M.J., Le Maitre, R.W., Streisen, A., Zanettin, B., 1986. A chemical classification of volcanic rocks based on the total alkali-silica diagram. J. Petrol. 27, 745–750. http://dx.doi.org/10.1093/petrology/27.3.745.

Bastow, I.D., Keir, D., Daly, E., 2011. The Ethiopia Afar Geoscientific Lithospheric Experiment (EAGLE): probing the transition from continental rifting to incipient seafloor spreading. In: Beccaluva, L., Bianchini, G., Wilson, M. (Eds.), Volcanism and Evolution of the African Lithosphere. Geological Society of America Special Paper 478. http://dx.doi.org/10.1130/2011.2478(04).

Blockley, S.P.E., Pyne-O'Donnell, S.D.F., Lowe, J.J., Matthews, I.P., Stone, A., Pollard, A.M., Turney, C.S.M., Molyneux, E.G., 2005. A new and less destructive laboratory procedure for the physical separation of distal glass tephra shards from sediments. Quat. Sci. Rev. 24, 1952–1960. http://dx.doi.org/10.1016/j.quascirev.2004.12.008.

Bronk Ramsey, C., 2009a. Bayesian analysis of radiocarbon dates. Radiocarbon 51 (1), 337–360.

Bronk Ramsey, C., 2009b. Dealing with outliers and offsets in radiocarbon dating. Radiocarbon 51 (3), 1023–1045.

Brown, F.H., 1982. Tulu Bor Tuff at Koobi Fora correlated to the Sidi Hakoma Tuff at Hadar. Nature 300, 631–635. http://dx.doi.org/10.1038/300631a0.

Brown, F.H., Haileab, B., IM, 2006. Sequence of tuffs between the KBS Tuff and the Chari Tuff in the Turkana Basin, Kenya and Ethiopia. J. Geol. Soc. 163, 185–204. http://dx.doi.org/10.1144/0016-764904-165.

Campisano, C., Feibel, C.S., 2008. The Geology of Early Humans in the Horn of Africa: Geological Society of America Special Paper 446. The Geological Society of America. Ch. Tephrostratigraphy of the Hadar and Busidima Formations at Hadar, Afar Depression, Ethiopia.

Clark, J.D., Beyene, Y., WoldeGabriel, G., Hart, W.K., Renne, P.R., Gilbert, H., Defleur, A., Suwa, G., Katoh, S., Ludwig, K.R., Boisserie, J.-R., Asfaw, B., White, T.D., 2003. Stratigraphic, chronological and behavioural contexts of Pleistocene *Homo sapiens* from Middle Awash, Ethiopia. Nature 423, 747–752. http://dx.doi.org/10.1038/nature01670.

Coussens, M., Wall-Palmer, D., Talling, P.J., Watt, S.F.L., Cassidy, M., Jutzeler, M., Clare, M.A., Hunt, J.E., Manga, M., Gernon, T.M., Palmer, M.R., Hatter, S.J., Boudon, G., Endo, D., Fujinawa, A., Hatfield, R., Hornbach, M.J., Ishizuka, O., Kataoka, K., Friant, A.L., Maeno, F., McCanta, M., Stinton, A.J., 2016. The

relationship between eruptive activity, flank collapse, and sea level at volcanic islands: a long-term >1(Ma) record offshore Montserrat, Lesser Antilles. Geochem. Geophys. Geosyst. 17 (7), 2591–2611. http://dx.doi.org/10.1002/2015GC006053.

Davies, S.M., 2015. Cryptotephras: the revolution in correlation and precision dating. J. Quat. Sci. 30 (2), 114–130. http://dx.doi.org/10.1002/jqs.2766.

Davies, S.M., Abbott, P.M., Pearce, N.J.G., Wastegård, S., Blockley, S.P.E., 2012. Integrating the intimate records using tephrochronology: rising to the challenge. Quat. Sci. Rev. 36, 11–27. http://dx.doi.org/10.1016/j.quascirev.2011.04.005.

DiMaggio, E.N., Campisano, C.J., Arrowsmith, J.R., Reed, K.E., Swisher, C.I.I., Lockwood, C.A., 2008. The Geology of Early Humans in the Horn of Africa: Geological Society of America Special Paper 446. The Geological Society of America, p. 163177. http://dx.doi.org/10.1130/2008.2446(07). Ch. Correlation and stratigraphy of the BKT-2 volcanic complex in west-central Afar, Ethiopia.

Feakins, S.J., Brown, F.H., deMenocal, P.B., 2007. Plio-pleistocene microtephra in DSDP site 231, Gulf of Aden. J. Afr. Earth Sci. 48, 341–352. http://dx.doi.org/10.1016/j.jafrearsci.2007.05.004.

Ferguson, D., Barnie, T.D., Pyle, D.M., Oppenheimer, C., Yirgu, G., Lewi, E., Kidane, T., Carn, S., Hamling, I., 2010. Recent rift-related volcanism in Afar, Ethiopia. Earth Planet. Sci. Lett. 292, 409–418. http://dx.doi.org/10.1016/j.epsl.2010.02.010.

Ferguson, D., Maclennan, J., Bastow, I.D., Pyle, D., Jones, S., Keir, D., Blundy, J., Plank, T., Yirgu, G., 2013. Melting during late-stage rifting in Afar is hot and deep. Nature 499, 70–73. http://dx.doi.org/10.1038/nature12292.

Field, L., Blundy, J., Brooker, R.A., Wright, T., Yirgu, G., 2012. Magma storage conditions beneath Dabbahu Volcano (Ethiopia) constrained by petrology, seismicity and satellite geodesy. Bull. Volcanol. 74, 981–1004. http://dx.doi.org/10.1007/s00445-012-0580-6.

Ghinassi, M., D'Oriano, F., Benvenuti, M., Awramik, S., Bartolini, C., Fedi, M., Ferrari, G., Papini, M., Sagri, M., Talbot, M., 2012. Shoreline fluctuations of Lake Hayk (northern Ethiopia) during the last 3500 years: geomorphological, sedimentary, and isotope records. Palaeogeogr. Palaeoclimatol. Palaeoecol. 365–366, 209–226. http://dx.doi.org/10.1016/j.palaeo.2012.09.029.

Goitom, B., Oppenheimer, C., Hammond, J.S., Grandin, R., Barnie, T., Donovan, A., Ogubazghi, G., Yohannes, E., Kibrom, G., Kendall, J.-M., Carn, S., Fee, D., CS, Keir, D., Ayele, A., Blundy, J., Hamlyn, J., Wright, T., Berhe, S., 2015. First recorded eruption of Nabro volcano, Eritrea, 2011. Bull. Volcanol. 77 (85) http://dx.doi.org/10.1007/s00445-015-0966-3.

Gouin, P., 1979. Earthquake History of Ethiopia and the Horn of Africa. International Development Research Centre, Ottawa.

Haile-Selassie, Y., Deino, A., Saylor, B., Umer, M., Latimer, B., 2007. Preliminary geology and paleontology of new hominid-bearing Pliocene localities in the central Afar region of Ethiopia. Anthropol. Sci. 115, 215–222. http://dx.doi.org/10.1537/ase.070426.

Jochum, K.P., Stoll, B., Herwig, K., Willbold, M., Hofmann, A.W., Amini, M., Aarburg, S., Abouchami, W., Hellebrand, E., Mocek, B., Raczek, I., Stracke, A., Alard, O., Bouman, C., Becker, S., Dücking, M., Brätz, H., Klemd, R., de Bruin, D., Canil, D., Cornell, D., de Hoog, C., Dalpé, C., Danyushevsky, L., Eisenhauer, A., Gao, Y., Snow, J.E., Groschopf, N., Günther, D., Latkoczy, C., Guillong, M., Hauri, E.H., Höfer, H.E., Lahaye, Y., Horz, K., Jacob, D.E., Kasemann, S.A., Kent, A.J.R., Ludwig, T., Zack, T., Mason, P.R.D., Meixner, A., Rosner, M., Misawa, K., Nash, B.P., Pfänder, J., Premo, W.R., Sun, W.D., Tiepolo, M., Vannucci, R., Vennemann, T., Wayne, D., Woodhead, J.D., 2006. MPI-DING reference glasses for in situ microanalysis: new reference values for element concentrations and isotope ratios. Geochem. Geophys. Geosyst. 7 (2), 1–44. http://dx.doi.org/10.1029/2005GC001060.

Kalnay, E., Kanamitsu, M., Kistler, R., Collins, W., Deaven, D., Gandin, L., Iredell, M., Saha, S., White, G., Woollen, J., Zhu, Y., Chelliah, M., Ebisusaki, W., Higgins, W., Janowiak, J., Mo, K.C., Ropelewski, C., Wang, J., Leetma, A., Reynolds, R., Jenne, R., Joseph, D., 1996. The NCEP/NCAR 40 year reanalysis project. Bull. Am. Meteorol. Soc. 77, 437–471. http://dx.doi.org/10.1175/1520-0477(1996)077<0437:TNYRP>2.0.CO;2.

Katoh, S., Nagaoka, S., WoldeGabriel, G., Renne, P., Snow, M.G., Beyene, Y., Suwa, G., 2000. Chronostratigraphy and correlation of the Plio-Pleistocene tephra layers of the Konso formation, southern Main Ethiopian Rift, Ethiopia. Quat. Sci. Rev. 19, 1305–1317. http://dx.doi.org/10.1016/S0277-3791(99)00099-2.

Keir, D., Belachew, M., Ebinger, C.J., Kendall, J.M., Hammond, J.O.S., Stuart, G.W., Ayele, A., Rowland, J.V., 2011. Mapping the evolving strain field during continental breakup from crustal anisotropy in the Afar Depression. Nat. Commun. 285 (2), 1–7. http://dx.doi.org/10.1038/ncomms1287.

Lamb, H.F., Leng, M.J., Telford, R.J., Ayenew, T., Umer, M., 2007. Oxygen and carbon isotope composition of authigenic carbonate from an Ethiopian lake: a climate record of the last 2000 years. Holocene 17 (4), 517–526.

Lane, C.S., Cullen, V.L., White, D., Bramham-Law, C.W.F., Smith, V.C., 2014. Cryptotephra as a dating and correlation tool in archaeology. J. Archaeol. Sci. 42, 42–50. http://dx.doi.org/10.1016/j.jas.2013.10.033.

Le Maitre, R.W., 2002. Igneous Rocks: A Classification and Glossary of Terms: Recommendations of the International Union of Geological Sciences Subcommission on the Systematics of Igneous Rocks. Cambridge University Press.

Mariner, R.H., Surdam, R.C., 1970. Alkalinity and formation of zeolites in saline alkaline lakes. Science 170, 977–980.

Marshall, M.H., Lamb, H.F., Davies, S.J., Leng, M.J., Kubsa, Z., Umer, M., Bryant, C., 2009. Climatic change in northern Ethiopia during the past 17,000 years: a diatom and stable isotope record from Lake Ashenge. Palaeogeogr. Palaeoclimatol. Palaeoecol. 279, 114–127. http://dx.doi.org/10.1016/j.palaeo.2009.05.003.

Mohr, P., 1978. Afar. Annu. Rev. Earth Planet. Sci. 6, 145–172. http://dx.doi.org/10.1146/annurev.ea.06.050178.001045.

Payne, R., Gehrels, M., 2010. The formation of tephra layers in peatlands: an experimental approach. Catena 81, 12–23.

Pearce, N.J.G., 1990. Zirconium and niobium-bearing ilmenites from the Igaliko dyke swarm, South Greenland. Mineral. Mag. 54, 585–588.

Pearce, N.J.G., Perkins, W.T., Westgate, J.A., Gorton, M.P., Jackson, S.E., Neal, C.R., Chenery, S.P., 1997. A compilation of new and published major and trace element data for NIST SRM 610 and NIST SRM 612 glass reference materials. Geostand. Newsl. 21, 115–144. http://dx.doi.org/10.1111/j.1751-908X.1997.tb00538.x.

Pearce, N.J.G., Bendall, C.A., Westgate, J.A., 2008. Comment on "Some numerical considerations in the geochemical analysis of distal microtephra' by A.M. Pollard, S.P.E. Blockley and C.S. Lane. Appl. Geochem. 23, 1353–1364. http://dx.doi.org/10.1016/j.apgeochem.2008.01.002.

Pearce, N.J.G., Perkins, W.T., Westgate, J.A., Wade, S.C., 2011. Trace-element microanalysis by LA-ICP-MS: the quest for comprehensive chemical characterisation of single, sub- ~10 μm volcanic glass shards. Quat. Int. 246, 57–81. http://dx.doi.org/10.1016/j.quaint.2011.07.012.

Peccerillo, A., Barberio, M.R., Yirgu, G., Ayalew, D., Barbieri, M., Wu, T.W., 2003. Relationships between mafic and peralkaline silicic magmatism in continental rift settings: a petrological, geochemical and isotopic study of the gedemsa volcano, central ethiopian rift. J. Petrol. 44 (11), 2003–2032. http://dx.doi.org/10.1093/petrology/egg068.

Peccerillo, A., Donati, C., Santo, A.P., Orlando, A., Yirgu, G., Ayalew, D., 2007. Petrogenesis of silicic peralkaline rocks in the ethiopian rift: geochemical evidence and volcanological implications. J. Afr. Earth Sci. 48 (2–3), 161–173. http://dx.doi.org/10.1016/j.jafrearsci.2006.06.010.

Pickford, M., Senut, B., Poupeau, G., Brown, F.H., Haileab, B., 1991. Correlation of tephra layers from the western Rift Valley (Uganda) to the Turkana Basin (Ethiopia/Kenya) and the Gulf of Aden. Comptes Rendus L'Académie Sci. Ser. II 313, 223–229.

Pyle, D.M., 1999. Widely dispersed quaternary tephra in Africa. Glob. Planet. Change 21, 95–112. http://dx.doi.org/10.1016/S0921-8181(99)00009-0.

Rawson, H., Naranjo, J.A., Smith, V.C., Fontijn, K., Pyle, D.M., Mather, T.A., Moreno, H., 2015. The frequency and magnitude of post-glacial explosive eruptions at Volcán Mocho-Choshuenco, southern Chile. J. Volcanol. Geotherm. Res. 299, 103–129. http://dx.doi.org/10.1016/j.jvolgeores.2015.04.003.

Reimer, P.J., Bard, E., Bayliss, A., Warren Beck, J., Blackwell, P.G., Bronk Ramsey, C., Buck, C.E., Cheng, H., Lawrence Edwards, R., Friedrich, M., Grootes, P.M., Guilderson, T.P., Haflidason, H., Hajdas, I., Hatté, C., Heaton, T.J., Hoffmann, D.L., Hogg, A.G., Hughen, K.A., Kaiser, K.F., Kromer, B., Manning, S.W., Niu, M., Reimer, R.W., Richards, D.A., Marian Scott, E., Southon, J.R., Staff, R.A., Turney, C.S.M., van der Plicht, J., 2013. IntCal13 and Marine13 radiocarbon age calibration curves 0-50,000 years cal BP. Radiocarbon 55 (4), 1869–1887. http://dx.doi.org/10.2458/azu_js_rc.55.16947.

Saylor, B.Z., Angelini, J., Deino, A., Alene, M., Fournelle, J.H., Haile-Selassie, Y., 2016. Tephrostratigraphy of the Waki-Mille area of the Woranso-Mille paleoanthropological research project, Afar, Ethiopia. J. Hum. Evol. 93, 25–45. http://dx.doi.org/10.1016/j.jhevol.2015.12.007.

Schilling, J.G., 1973. Afar mantle plume: rare earth evidence. Nature 242, 2–5. http://dx.doi.org/10.1038/physci242002a0.

Siebert, L., Simkin, T., Kimberly, P., 2011. Volcanoes of the World, third ed. University of California Press.

Sparks, R.S.J., Bursik, M.I., Carey, S., Gilbert, J.G., Glaze, L.S., Sigurdson, H., Woods, A., 1997. Volcanic Plumes. John Wiley & Sons.

Tomlinson, E.L., Albert, P.G., Wulf, S., Brown, R.J., Smith, V.C., Keller, J., Orsi, G., Bourne, A.J., Menzies, M.A., 2014. Age and geochemistry of tephra layers from ischia, Italy: constraints from proximal-distal correlations with lago grande di monticchio. J. Volcanol. Geotherm. Res. 287, 22–39.

Ukstins Peate, I., Baker, J.A., Kent, A.J.R., Al-Kadasi, M., Al-Subbary, A., Ayalew, D., Menzies, M., 2003. Correlation of Indian Ocean tephra to individual Oligocene silicic eruptions from Afro-Arabian flood volcanism. Earth Planet. Sci. Lett. 211, 311–327.

Watson, E.B., 1979. Zircon saturation in felsic liquids - experimental results and applications to trace-element geochemistry. Contrib. Mineral. Petrol. 70, 407–419. DOI: 10.1007%2FBF00371047.

Wiart, P., Oppenheimer, C., 2000. Largest known historical eruption in Africa: Dubbi volcano, Eritrea, 1861. Geology 28 (28), 291–294. http://dx.doi.org/10.1130/0091-7613(2000)28<291:LKHEIA>2.0.CO;2.

Wiart, P., Oppenheimer, C., 2004. Large magnitude silicic volcanism in north Afar: the Nabro Volcanic Range and Ma'alalta volcano. Bull. Volcanol. 67, 99–115. http://dx.doi.org/10.1007/s00445-004-0362-x.

WoldeGabriel, G., Walter, R.C., Hart, W.K., Mertzman, S.A., Amd Aronson, J.L., 1999. Temporal relations in the geochemical features of felsic volcanism in the central sector of the Main Ethiopian Rift. Acta Vulcanol. 11 (1), 53–67.

Wulf, S., Kraml, M., Brauer, A., Keller, J., Negendank, J.F.W., 2004. Tephrochronology of the 100ka lacustrine sediment record of Lago Grande di Monticchio (southern Italy). Quat. Int. 122, 7–30.